SAPIENZA
UNIVERSITÀ DI ROMA

Department of Physiology and Pharmacology

PhD in Neurophysiology XXVI cycle

Role of behavioral state in linear estimation of local field potentials

Valeria d'Andrea

December 2013

Tutor:
Prof. Stefano Ferraina
Department of Physiology and Pharmacology
"Sapienza" University of Rome

Contents

1. Introduction

To a large extent, one of the main purposes of neuroscience is to study how sensory, motor and cognitive processes are coded by neurons. One approach to these questions comes from the study of neural activity recorded through extracellular micro electrodes implanted in animal brains, which record action potentials, or spikes, emitted by neurons in a specific brain area around the electrode tip.

From recordings it is possible to discriminate the activity of single neurons through methods generally called "spike sorting" (Quiroga, Nadasdy et al. 2004). Much of what today is known about brain functional organization comes from studies on single-unit activity, and several works reported that spiking activity in specific brain areas correlates with sensory, motor and cognitive aspects of behavior (Rees, Kreiman et al. 2002; Buzsáki 2006; Grün and Rotter 2010).

However, single-unit activity offers a relatively narrow window into neural processing: the latter is believed to be the outcome of the concerted activity of large populations of neurons, so that even with today's impressive ability to record spikes from tens electrodes, single-unit activity represents a drastic undersampling of a collective dynamic phenomenon. Therefore it would be obviously desirable to gain access to 'population signals'. In this perspective, recently much interest arose in the components of the signal recorded from the extracellular electrode which, for the purpose of discriminating single-unit activity, were just dismissed as noise. Before defining such population signals, whose relation with single unit activity is one focus of the present thesis, we emphasize that the problem is not just a technical one of identifying a convenient probe to 'sense' the activity of many neurons around the electrode; decades of electrophysiology proved that even in small regions of the cortex the specific computational role of single neurons can be very different (different selectivity in sensory areas, different coding properties in areas devoted to memory, etc). Therefore, whether by gathering population signals one is indeed providing better sampling of the activity of neurons with coherent functions, or one is averaging out heterogeneous selectivity, thus loosing information, remains to be understood and assessed on a case by case basis.

The voltage recorded extracellularly through electrodes is typically separated in two frequency bands. The high-frequency part (above about 500 Hz) is called multi-unit activity (MUA) and represents a weighted sum of the spiking activity of a neural population, in a sphere with radius of about 200 μm, located around the electrode tip (Logothetis, Pauls et al. 2001; Buzsáki 2006; Stark and Abeles 2007).

Low-pass filtering the extracellular signals with a cutoff frequency of about 200 Hz yields the local field potential (LFP). Several studies attested that LFP could convey information on perception and cognition of the subject. Some works attested that LFP is linked to sensory stimuli coding, reporting that signals recorded in visual cortex are tuned for speed and directions of simple point stimuli (Liu and Newsome 2006) and contain information about rich naturalistic stimuli (Belitski, Gretton et al. 2008). Other works reported a significant increase of LFP power in working memory tasks (Pesaran, Pezaris et al. 2002) and in attentional selection, which was found to enhance γ frequency band ([30 80] Hz) synchrony and to suppress δ ([1 3] Hz) and θ ([4 8] Hz) bands (Schroeder and Lakatos 2009).

The role of LFP was also studied in experiments of functional magnetic resonance imaging (fMRI), which use BOLD signal (blood oxygen level) to infer neurons activity in a specific cortical area: it was reported that the prediction of BOLD response from LFP is more accurate than that obtained from spiking activity (Logothetis, Pauls et al. 2001).

The biophysical origin of LFP is difficult to interpret. For several years, investigators stressed the role of synaptic activity in the generation of LFP, which would mostly represent a weighted average of synchronized dendro-somatic components in a wide region (up to few millimetres) around the electrode tip (Mitzdorf 1987; Logothetis, Pauls et al. 2001). The spatial extent of the cortical region which contributes to the recorded LFP is still debated: several studies showed that a typical spatial scale for both the origin and the specificity of LFP would be fairly local - up to 200 μm around the recording site (Katzner, Nauhaus et al. 2009) while other studies found much larger numbers for such scales, as mentioned above . A recent modeling study showed that these results can be reconciled by assuming that the spatial extent of LFP strongly depends on the amount of correlation of neural LFP sources: for uncorrelated synaptic LFP sources it is about 200

μm, whereas, correlated synaptic inputs generate a "constructive interference" effect which increases LFP effective spatial scale (Einevoll, Kayser et al. 2013).

Moreover, in recent years, several works examined the relationship between LFP and spiking activity, and attested that other signals which contribute to LFP come from spike afterpotentials and somatodendritic spikes (Ray and Maunsell 2011). That scenario is unsurprising if we consider the structure of a typical neural network, a structure where over 60% of connections remain local and generate synaptic activity in the same cortical region (Rainer 2008). In this scheme LFP are influenced both from synaptic inputs from remote cortical areas and from processing of the local spikes, including the activity of excitatory and inhibitory interneurons.

In the present work we investigate the dependence of LFP on spiking activity and how this relationship can be influenced by experimental conditions (such as a motor task or behavioral state of the animal) which likely involve different neural populations and different correlations between spiking activity and LFP. Motivated by the success of a similar approach in simpler contexts and in anesthetized animals (Rasch, Logothetis et al. 2009), to accomplish this we use a simple linear approach, in which the LFP is just expressed as a convolution of the spike sequence (or the MUA) with a kernel, the latter being determined by a criterion of optimal reconstruction. We found that phase relationships between spikes and LFP at frequencies below 40 Hz are determinant to understand linear dependence. This is consistent with other studies (Rasch, Gretton et al. 2008) according to which phase and power of LFP in lower frequency band (<10 Hz) are significant predictors of spiking activity, together with LFP power in high ([40 90] Hz) band.

We also found that, further disentangling signals that hypothetically result from different neural populations which are involved in a given behavioral task, we can improve the kernel estimation for the assumed linear dependence of LFP on spiking activity. For example, dealing with separate classes of putative excitatory and inhibitory neurons, studying separately the LFP phase at which spikes are emitted, can increase the fraction of LFP estimated from spiking activity.

2. Materials and methods

2.1. Electrophysiological recording and data preprocessing

Two male monkeys (Macaca mulatta, L e S) partecipated in these experiments in accordance with European guidelines (European Community Council Directive 86/609/ECC) and with Italian national law (DL 116/92) on the use of animals in research.

General procedures were described recently (Mirabella, Pani et al. 2011; Mattia, Pani et al. 2013). Briefly, on each monkey, a chronic recording chamber (18mm inner diameter) was stereotaxically implanted over the left frontal cortex (coordinates A16, L12) in order to have the arm representation of the dorsal premotor cortex (PMd) within the explored region (Fig. 1).

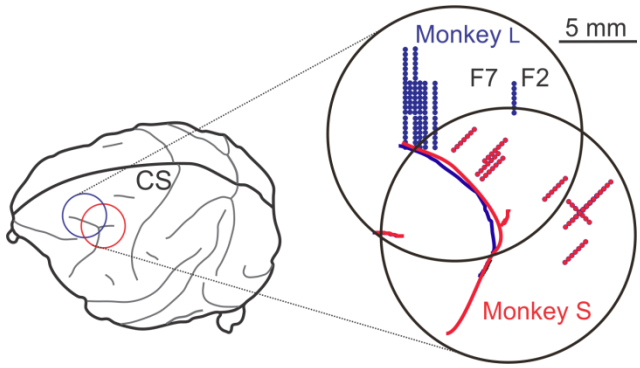

Fig.1. Recording sites in PMd. Left: a schematic representation of recording chambers position on a macaque brain picture for both the animals involved in the experiments. Position of central sulcus, CS, is reported. Right: position of the recording chambers and electrodes for both monkeys L and S. Penetrations ranged between the rostral (F7) and caudal (F2, PMd) part of PMd. Inside each chamber, lines show the position of arcuate sulcus.

Monkeys were placed in a darkened chamber, with head fixed, facing a 21" monitor equipped with a touch screen (Micro Touch, sampling rate 200 Hz). A free open-source software package, CORTEX (dally.nimh.nih.gov), was used to control stimuli and behavior. During recordings, quartz-insulated platinum-tungsten electrodes (80 µm outer diameter, impedance 0.8−2.5MΩ) were inserted transdurally in the explored region through a seven electrodes microdrive (Thomas Recording, Giessen, Germany). The raw

signal from each electrode was continuously sampled during the entire session (TDT Tucker-Davis technologies: Sampling rate 24,414 Hz; High-pass filter: 0.1 Hz).

Animals were trained to perform a reaching version of the stop-signal task or countermanding task (Logan, Cowan et al. 1984) (Fig. 2). All trials started with the appearance of a central target the monkeys have to touch with their right hands within 1000 ms. After a variable (500-800 ms) the central target disappeared and simultaneously a peripheral target (Go signal) appeared at one of two opposite positions with respect to the center (movement conditions, left and right). In Go trials, the monkey had to reach the target within a maximum allowed time (reaction time (RT) of 600 ms for monkey L and 750 ms for monkey S) in order to obtain reward. One randomized fraction of trials (33%; Stop trials), central cue reappeared during RT, instructing the monkey to inhibit movement initiation. Stop signal delays varied randomly to allow the animals to inhibit about half of the Stop trials (Correct Stop trials). No reward was delivered, when the monkey started the movement despite the Stop signal (Wrong Stop trials).

We considered four trial's epochs that correspond to different behavioural states. The Inter Trial epoch (IT) is 600 ms time interval before the appearance of the central target during which the monkey does not receive any stimulus. A 200 ms time interval (Movement) is selected during the arm movement, precisely from the hand central detouchment to the following peripheral touch of the screen. The Cue Expectation epoch is a 600 ms time interval between the appearance of the central target and the Go signal. Finally, the Reward Expectation epoch is selected in Go trials, and it refers to the epoch which starts with the peripheral touch of the screen, at the end of a movement.

Because different epochs have different time durations, we performed the analysis by dividing the 600 ms intervals in three segments of 200 ms and by averaging the results obtained in each segment.

Throughout the text, we performed the analysis in each of the four trial epochs (Inter Trial, Movement, Cue Expectation and Reward Expectation). Results obtained in Inter Trial and Movement epochs are averaged across daily data recording sessions and electrodes (18 sessions, 61 electrodes for monkey L and 12 sessions, 50 electrodes for monkey S), movement conditions (left and right) and monkeys. Monkey L and S gave different results in Cue Expectation and in Reward Expectation epochs, so in present work results in these time intervals cannot be averaged and are shown separately for each monkey.

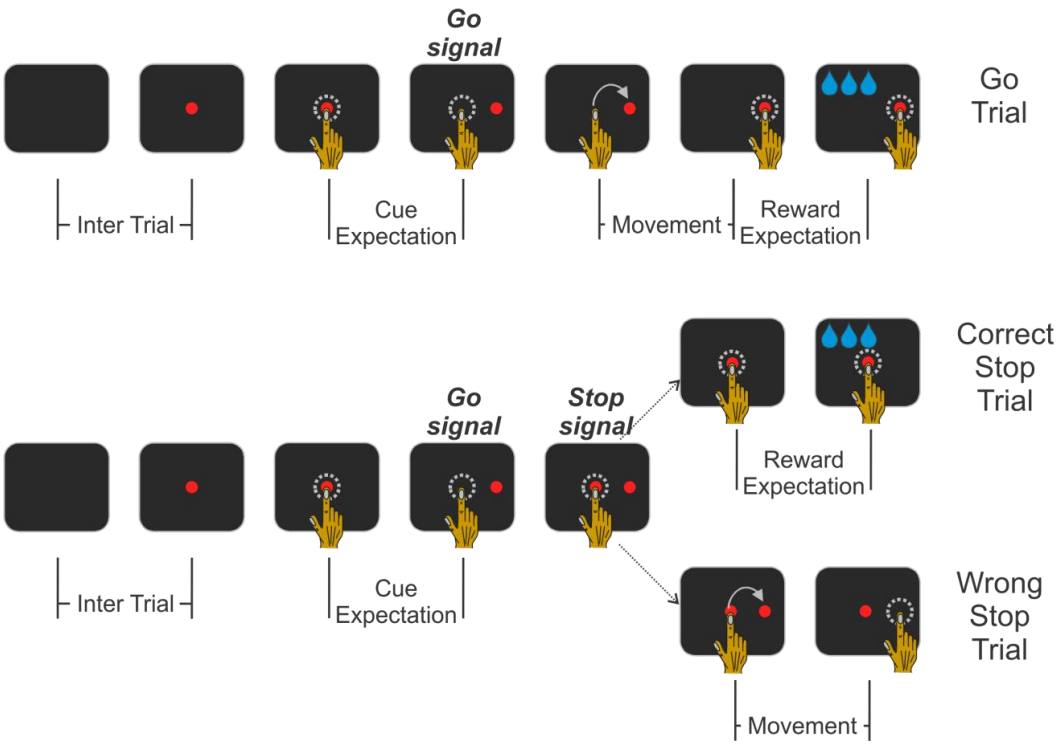

Fig.2. Countermanding task description. Temporal sequence for Go and Stop trials. All trials began with the presentation of a central cue to be touched by the monkey. After a variable holding time peripherical cue appeared (go signal) at one of two opposite directions from the central cue (right or left). In Go trials monkey had to start a reaching movement toward the target in order to obtain reward. In Stop trials the central cue reappeared (stop signal) instructing the monkey to inhibit movement initiation. If monkey withheld the arm obtain reward (correct Stop trial). No drops of juice were delivered when monkey executed the reaching movement ignoring the stop signal (wrong Stop trial). In each trial were selected four time epochs that correspond to different behavioral states: Inter Trial (IT), during which monkey does not have any visual stimuli, Movement, and two different epochs related to attention, when monkey is holding his arm on the screen and is waiting for go signal (Cue Expectation) or reward (Reward Expectaion).

Some data preprocessing steps were performed in order to obtain local field potentials (LFP), spike times and multi unit activity (MUA).

Electrode raw signals were downsampled at 8.138 kHz. The LFP were extracted by band-pass-filtering the 8 kHz signals with a 4^{th} order Butterworth filter in the frequency range [1 220] Hz. Forward and backward filtering was used for the elimination of phase shifts introduced by the filters. The LFP signals were again downsampled to a rate of 508 Hz to increase the speed of the processing.

Spike times were detected by high-pass filtering the by 8 kHz signal (4^{th} order Butterworth filter, cutoff frequency of 508 Hz) and by performing an upwards amplitude

thresholding. The detection threshold was set according to previous studies (Quiroga, Nadasdy et al. 2004):

$$Thr = 4\sigma_n; \qquad \sigma_n = median\left\{\frac{|x|}{0.6745}\right\}$$

where x is the high-pass-filtered signal. Thus, the spikes used for the analysis represent the spiking activity of a small population of neurons rather than well separated spikes from a single neuron. Afterwards in this text (*Spike sorting and neuron classes*) a spike sorting analysis is performed, but, unless otherwise stated, the results must be considered as obtained with these unsorted spikes.

MUA estimation has been described in detail previously (Mattia, Pani et al. 2013). Briefly we computed the time-varying power spectra $P(f,t)$ from the short time Fourier transform of raw signal in 2 ms sliding windows. Relative spectra $R(f,t)$ were obtained by normalizing $P(f,t)$ by their average $P_{IT}(f)$ across the IT epoch. Then, we averaged $R(f,t)$ across the frequency band [508 2000] Hz in order to obtain a signal in the time domain. For comparison purpose, we estimated MUA also according to another work (Stark and Abeles 2007) and we found consistent results.

2.2. Linear LFP estimation

In a recent work (Rasch, Logothetis et al. 2009), Rasch and coworkers found that a significant fraction of LFP could be explained through a linear filter operation on the activity of few neurons. Using a signal recorded from the primary visual cortex (V1) of anesthetized monkeys, they found a surprising generality of these filters across different stimuli, electrode locations and animals. In the present work we applied the same methods to a signal recorded the dorsal premotor cortex (PMd), in different epochs of a countermanding task performed by awake monkeys. Different aspects were examinated: first we test the accuracy of a linear estimation in a cortical area, the PMd, that is involved in the control of a movement as well as in more abstract cognitive functions, such as inhibitory control(Mirabella, Pani et al. 2011) and attention (Boussaoud 2001). Another important aspect we want to inspect is to test linear estimation analysis in multiple epochs of the task which correspond to different behavioral state of the awake

monkey. Finally,we test LFP estimation accuracy by performing the analysis not only with spikes from a limited numbers of neurons but also with MUA which reflects the spiking activity in a wider cortical area.

Methods of estimation theory (Poor 1994; Gabbiani and Koch 1996) were used to gain insights on the relationships between LFP and spiking activity. According to these methods it is possible compute a temporal filter $K(t)$ that , when convolved with the spike train of the neuron, will produce an estimate $LFP_{\mathrm{est}}(t)$ of $LFP(t)$. In other words, it is possible to reconstruct part of the time-course of the LFP from the spike trains. It was also attested that some properties of the spike trains can influence the choice of the optimal method to compute $K(t)$. For example, it was demostrated(Gabbiani and Koch 1996) that, in the limit of low firing rates, the optimal filters coincide with a spike-triggered-average(STA) of LFP. In our work we preferred use a general method which is not affected by assumption on the spike times features to compute $K(t)$, that is a Wiener-Kolmogorov(W-K) filter.

To avoid overfitting the data,we used half of the trials recorded from each electrode to compute the W-K filter $K_{\mathrm{LFP}}(\mathrm{t})$ and computed the estimated signal $LFP_{\mathrm{est}}(t)$ by convolving $K_{\mathrm{LFP}}(\mathrm{t})$ with the second half of the trials. We performed analysis using as $x(t)$ both the spike times and MUA. $K_{\mathrm{LFP}}(\mathrm{t})$ is the inverse Fourier transform of the ratio of the cross-correlation, $\mathrm{P}_{\mathrm{LFP}-x}$, between the LFP and $x(t)$ and the autocorrelation, P_{x-x} , of $x(t)$:

$$K_{\mathrm{LFP}}(\mathrm{t}) = \int_{-\mathrm{f_c}}^{\mathrm{f_c}} \frac{\mathrm{P}_{\mathrm{LFP}-x}(\mathrm{f})}{\mathrm{P}_{x-x}(\mathrm{f})} \mathrm{e}^{-2\pi \mathrm{ift}} d\mathrm{f}$$

where f_c is the cutoff frequency of LFP, 220 Hz. The spectral analysis was computed with a fast Fourier transform algorithm and Bartlett windowing using nfft=2048.

We used the second half of the trials to estimate LFP:

$$LFP_{\text{est}}(t) = \int_0^T \text{x}(t-\tau) K_{\text{LFP}}(\tau)\, d\tau$$

where T=200 ms.

When performing linear estimation with spike times we excluded from the analysis trials with mean firing rate below 5 Hz. To measure the estimation performance we computed the Pearson's correlation coefficient (r, Estimation Accuracy) between LFP and its linear estimate. We evaluated the statistical significance of Estimation Accuracy by estimating LFP from a random signal. In case of linear estimation with spike times, we generated random spike times with the same mean firing rate of the experimental ones and Poisson distribution. Where W-K filters are obtained with MUA, we tested the statistical significance by generating a white noise signal with the same mean and standard deviation of the experimental MUA.

2.3. Phase of LFP at spike times

W-K filters show all activity that is locked to spikes. The components of LFP that are captured by the filters can be divided in two groups: events strictly associated to the spikes, with time extents tipical of the spike duration (under 5 ms) and all network oscillations which are phase locked to spike times, that will be captured in the W-K filter if spikes occur preferentially at certain phases of LFP.

To study the distribution of phases at spikes times across all LFP frequency, we computed a band-limited LFP by filtering forward backward LFP with a 4^{th} order Butterworth filter with bandwidth step of 5 Hz in the frequency range [5 220] Hz. From these band-passed signals, we computed the instantaneous phase as the argument of the Hilbert transform (Montemurro, Rasch et al. 2008). The sinusoidal convention used for phase is cosine type, so the phase values at 0 and π correspond respectively to the peak and trough of the oscillation. For each channel and frequency band, we computed the distribution of spike times as a function of the band-passed LFP phase, where the phase range $[0\ 2\pi]$ is binned with $\pi/16$ step. We computed the normalized spike times

distribution, P_s, by dividing each bin value by the sum over the bins, so that the integral of P_s over the whole phase range is one. According to (Tort, Komorowski et al. 2010) we defined the Modulation Index (MI) as a measure that quantifies the deviation of P_s from the uniform distribution:

$$MI = \frac{\log_2 N - H(P_s)}{\log_2 N}$$

where N is the number of phase bins and $H(P_s)$ is the Shannon entropy of the distribution, defined by:

$$H(P_s) = -\sum_{j=1}^{N} P_s(j) \log_2 P_s(j)$$

Normalizing the distance between P_s and the uniform distribution by the maximum entropy value ($H(P) \leq \log_2 N$) makes MI assume values between 0 and 1. We performed a statistical control analysis to test if the MI value differs from what would be expected from chance. To infer the MI chance distribution we generated 100 surrogate MI values by associating the spike times of trial k to the phase of band-passed LFP of trial l, with k and l randomly chosen among the trial numbers. A MI was considered statistically significant if it exceeds $(1 - p)\%$ of the surrogate values ($p = 0.01$).

If the MI of a normalized spike times distribution P_s is statistically significant, we estimated the parameters of the distribution and used them to assess the number of modes. The von Mises is a fundamental distribution that arises naturally for circular data, akin to the Normal distribution. The density function of the von Mises distribution is given by:

$$f(\theta) = \frac{1}{2\pi I_0(k)} e^{-k\cos(\theta-\mu)}$$

where μ represents the preferred phases of the population θ , k is the concentration parameter that indicates how closely θ clusters around μ and $I_0(k)$ denotes the modified Bessel function of the first kind and order 0. A mixture of two von Mises can be represented by the density function:

$$f(\theta) = p\frac{1}{2\pi I_0(k_1)} e^{-k_1\cos(\theta-\mu_1)} + (1-p)\frac{1}{2\pi I_0(k_2)} e^{-k_2\cos(\theta-\mu_2)}$$

where μ_1 and k_1 represent the vector mean and concentration parameter of the first component, similarly for μ_2 and k_2 of the second component, and p represents the proportion (fraction) of component 1 in the entire distribution. We tested two different methods to estimate the five parameters. A method-of-moments estimation procedure that was proposed by Spurr (Spurr and Koutbeiy 1991) and by Jones (Jones 2006), and method-of-minimum-distance estimation proposed by Spurr (Spurr and Koutbeiy 1991). Both methods produced similar results in the parameters estimation.

Once that the parameters of the normalized spike times distribution *P* were estimated, we examined the numbers of modes of the distribution. Mardia (Mardia and Sutton 1975; Holzmann and Vollmer 2008) gave precise conditions for unimodality or bimodality in terms of these parameters. Study the number of modes of the distribution can be useful to infer if all neurons have the same preferred phase with respect to the LFP, or if, otherwise, spikes tend to clusterize according to multiple phases, which can suggest the interplay of different neural sub-population during the epoch of the task.

2.4. Phase-amplitude coupling

The interaction of rhythms in different frequency bands is called cross-frequency coupling. In phase-amplitude coupling, also called nesting, the amplitude of high frequency oscillation is modulated by the phase of low frequency rhythms. Phase-amplitude coupling has been suggested to be involved in attentional selection (Schroeder and Lakatos 2009) and in memory process (Fell and Axmacher 2011).

As described previously, we computed the instantaneous phase of band-limited LFP. For each electrode and LFP frequency band, we computed the distribution of MUA amplitudes as a function of LFP phase, where the phase range $[0\ 2\pi]$ is binned with $\pi/16$ step, by mediating MUA amplitudes in each phase bin. We computed the normalized amplitude distribution, P_a, by dividing each bin value by the sum over the bins, so that the integral of P_a over the whole phase range is one. We computed the MI to quantify the deviation of P_a from the uniform distribution. To asses statistical significance of MI we generated 100 surrogate MI values by associating the MUA of trial k to the phase of band-passed LFP of trial l, with k and l randomly chosen among the trial numbers. A MI was considered statistically significant if it exceeds $(1-p)\%$ of the surrogate values ($p = 0.01$). If P_a is significantly different from the uniform distribution, we estimated parameters and number of modes of the distribution, as stated above.

2.5. Spike sorting and neuron classes

To better understand the relationship between local firing activity and LFP we sorted spikes, previously obtained with a threshold procedure, assigning them to putative single neurons. Then we classified neurons in two different groups according to the time duration of their action potentials, in order to study how phase of firing of different classes of PMd neurons depends on the trials epoch.

To extract spike waveforms we high-pass filtered the signal at 24.4 kHz sampling rate with a 4th order Butterworth filter in the frequency range [500 4000] Hz, we mediated to

zero and we selected the signal in a time interval of 2.6 ms around (0.8 ms before and 1.8 ms after) each spike time previously obtained.

To compute spike sorting we used free software Wave_Clus (Quiroga, Nadasdy et al. 2004). Not all putative neurons were used for further analysis: we rejected automatically neurons with at least 5% of inter-spike-intervals less than 3 ms. Then we separated out by visual inspection neurons with mean waveform which were very flat or not canonical (e.g. lacking a trough or a post-trough peak).

For each neuron, all recorded waveforms were aligned by their troughs and averaged. According to other works (Mitchell, Sundberg et al. 2007; Song and McPeek 2010) we used the trough to align action potentials because it was generally the sharpest feature of the waveform and was thus less sensitive to noise than the peak. The average waveform then was interpolated by a spline to give a temporal precision of 2.5 μs.

We defined waveform widths as the time interval from the trough to the peak (ttp) of the average action potential. We selected this measure on the basis of previous studies (Mitchell, Sundberg et al. 2007; Kaufman, Churchland et al. 2010; Song and McPeek 2010) showing that ttp interval can better distinguished broad-spiking pyramidal neurons from narrow- fast-spiking interneurons.

We examinated the distribution of spike widths to determine wheter it was bimodal and could therefore be divided into narrow- and broad-spiking neuron classes. For each monkey and for the overall (both monkeys) distributions we found a significant bimodality according to Hartigan' s dip test ($p<0.01$) (Hartigan 1985). Hartigan's test was computed with free matlab codes avaible on line (http://www.nicprice.net) which compute statistical significance with a bootstrap sample of size N=500 of the dip statistic for a uniform distribution of sample size the same as empirical distribution. Narrow- and broad- spiking neurons were separated on the basis of the two modes of the distribution, with narrow- spiking neurons defined as those with ttp interval in range [200 400] μs and broad-spiking neurons defined as those with ttp range [401 900] μs.

3. Results

2.1. Linear estimation of LFP from spikes and MUA

We estimated LFP from spikes and MUA. We based the first part of our analysis on the recent work of Rasch and coworkers (Rasch, Logothetis et al. 2009) who found that a significant fraction of LFP can be inferred through a linear filter operation on the spiking activity of neurons around the electrode tip. Rasch's analysis was computed on data recorded from the primary visual cortex of anesthetized monkeys and results claimed a surprising generality of filters across different stimuli, electrode locations and animals. In this work we applied the same methods to our data to test both the validity of LFP linear estimation and the invariance of linear filters shapes in trial epochs corresponding to different behavioral states.

We considered activity of 111 electrodes (61 electrodes collected during 18 daily sessions for monkey L and 50 electrodes in 12 sessions for monkey S) recorded from PMd of two monkeys performing a countermanding task. We analyzed 4402 Go trials, where a movement is performed without inhibition, 1216 Correct Stop trials, where the required inhibition is correctly performed and 988 Wrong Stop trials, where a movement is performed even though a cue requiring inhibition is presented.

We chose to focus our analysis on four trial epochs: Inter Trials, Movement, Cue Expectation and Reward Expectation. If, in a specific trial, the minimum duration of each epoch (200 for Movement, 600 ms for the other epochs) is not fulfilled, we excluded that trial from our analysis.

The Inter Trial and Movement epochs produce results, which are very similar across monkeys, both in Estimation Accuracy of LFP, shapes of W-K filters and, as showed later, also in phase relationships between LFP and spiking activity. According to these findings, we averaged results across monkeys in these epochs. Monkey L and S gave different results in Cue Expectation as well as in Reward Expectation epochs, so in present work results in these time intervals cannot be averaged and are shown separately for each monkey. Differences in behavioral data of ocular and arm movements recorded during the task, as previously described in previous paper (Mirabella, Pani et al. 2011), suggest that the two animals used two different strategies to perform the countermanding

task: monkey L carried out a faster eye/arm movement towards the cue, whereas monkey S did not move eyes from the center of the screen, waiting for the stop signal, and displayed very long reaction times. These different plans of actions can take into account of the differences in Cue Expectation epoch that can be so related to different level of attention that the two monkeys involved in the wait of the target. More difficult to interpret in terms of behavior and attention involved are the differences in our results regarding Reward Expectation epoch, even if a different arousal level can be hypothesized to be involved also in the wait of reward delivery.

Our analysis was computed by linear filtering LFP with both punctual spike trains and continuous MUA, the latter likely measuring the spiking activity of a larger neural population around the electrode tip. In order to better describe the differences between the two used signals, in Figure 3 we show two examples, from signals recorded in two random trials, of linear estimation of LFP obtained with MUA (top) and spike trains (bottom), which are shown, respectively, as blue line and blue vertical ticks. Black line is LFP and red line is the estimated LFP. We also reported the Pearson's correlation coefficient (r, Estimation Accuracy) between LFP and its linear estimate.

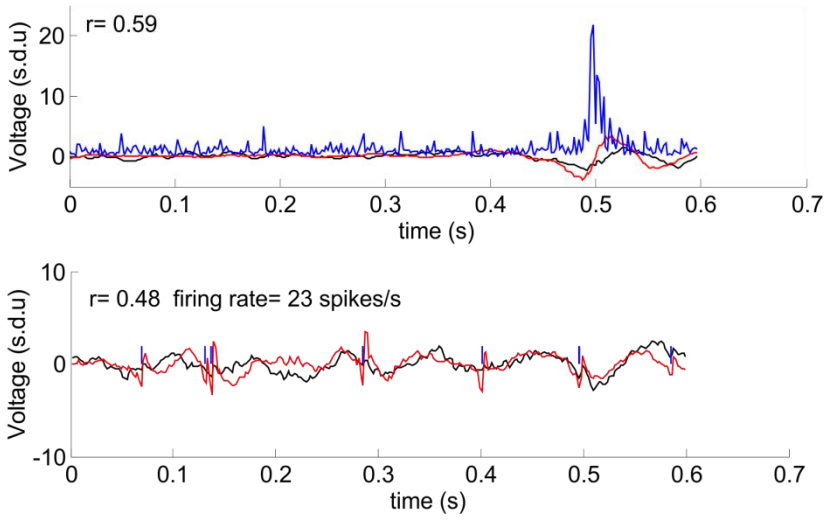

Fig. 3. Linear estimation of LFP, in two random trials, obtained with MUA (top, blue line) and spikes (bottom, blue vertical ticks). LFP and its estimate are shown as, respectively, black and red lines. We also reported the Pearson's correlation coefficient (r, Estimation Accuracy) between LFP and its linear estimate, and mean firing rate for spikes.

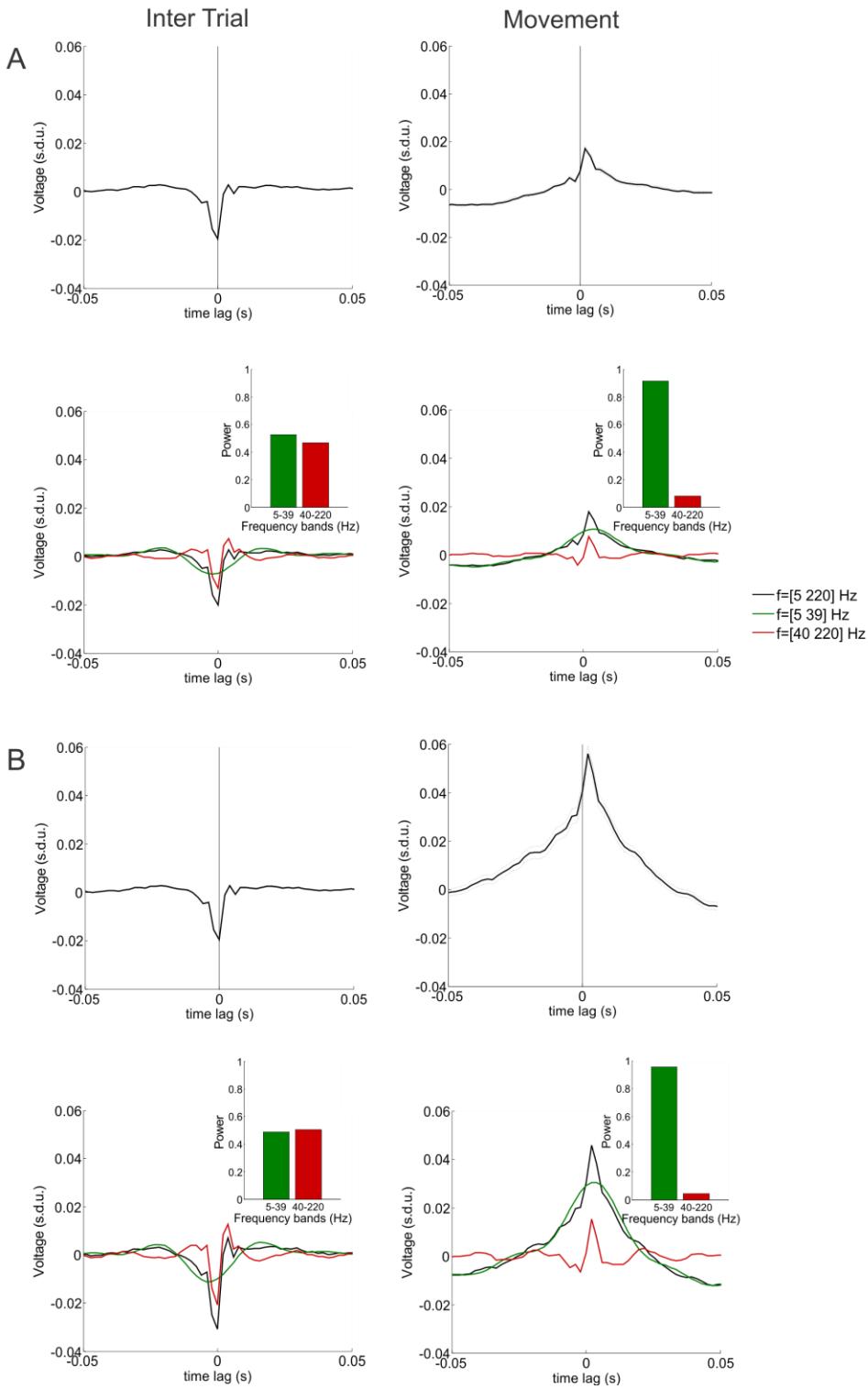

Fig. 4. Averages across all electrodes and monkeys of W-K linear filters obtained with MUA (Fig. 4A) and spike trains (Fig. 4B), in Inter Trial (left) and Movement (right) epochs of the trial. For each electrode, half of the trials were used to compute the W-K filters. Green lines: component of W-K kernel obtained by filtering in [5 39] Hz frequency range; red lines: component of W-K filter in [40 220] Hz. Inset bar plots: power of the two components of the filter, normalized to the power of unfiltered kernel.

Figure 4 shows W-K linear filters obtained with MUA (Fig. 4A) and spike trains (Fig. 4B), in Inter Trial (left) and Movement (right) epochs of the trial. Results from spike trains and MUA are strongly consistent.

First row shows the average and SEM across both monkeys, all electrodes and movement conditions (left and right). Figures show that filters remarkably depend on the trial epoch.

As previously noted, two different biophysical sources can contribute to W-K filter: a fast component of LFP, related to the spike waveform and its time duration, and a slow component of LFP, related to the network oscillations which are phase locked to the spikes times. According to other works (Ray, Hsiao et al. 2008) we found that the components that mostly compose the filter are the oscillations in the low frequency range (up to 40 Hz) and a waveform in a high frequency range (over 200 Hz), whereas LFP components in γ and high-γ bands do not seem to affect the filter. To simply describe differences between flters in multiple epochs of the task, we filtered the average W-K kernel in two frequency ranges, a low frequency band of [5 39] Hz and a high frequency band of [40 220] Hz, showed respectively in green and red in the second rows of the figures. These frequency bands mainly represent the two different biophysical sources that form W-K filter.

We also computed the power in each frequency band by integrating the square of each band-passed kernel over time (according to the Parseval's theorem this is equal to power in frequency domain), and normalizing to the power of unfiltered kernel (in the inset). We found that W-K filter varies significantly across different epochs, with a Movement kernel strongly modulated in the low frequency band respect to the IT.

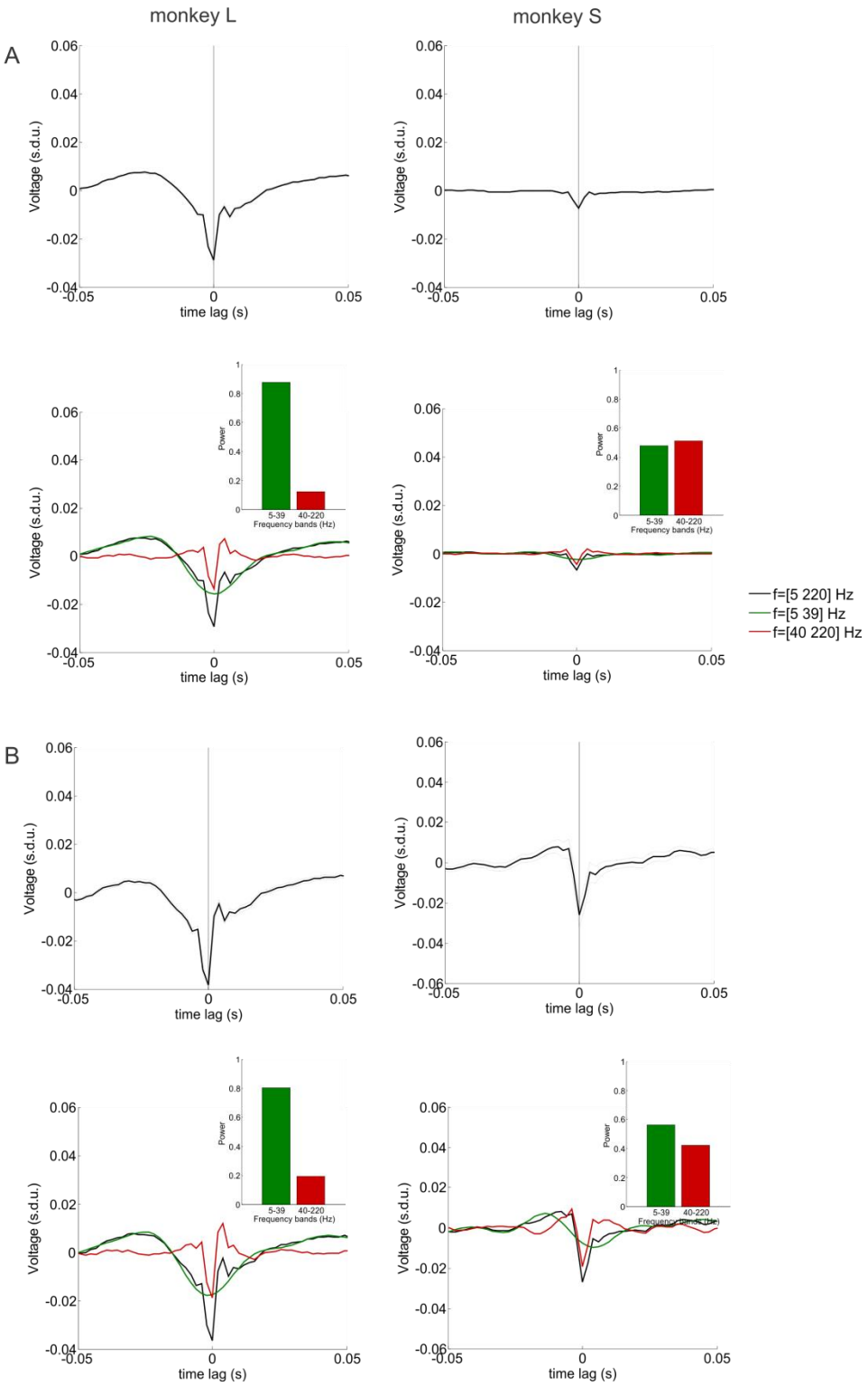

Fig. 5. Averages across all electrodes of W-K linear filters obtained with MUA (Fig. 5A) and spike trains (Fig. 5B), in Cue Expectation epoch, for monkey L (left) and monkey S (right). Green lines: component of W-K kernel obtained by filtering in [5 39] Hz frequency range; red lines: component of W-K filter in [40 220] Hz. Inset bar plots: power of the two components of the filter, normalized to the power of unfiltered kernel

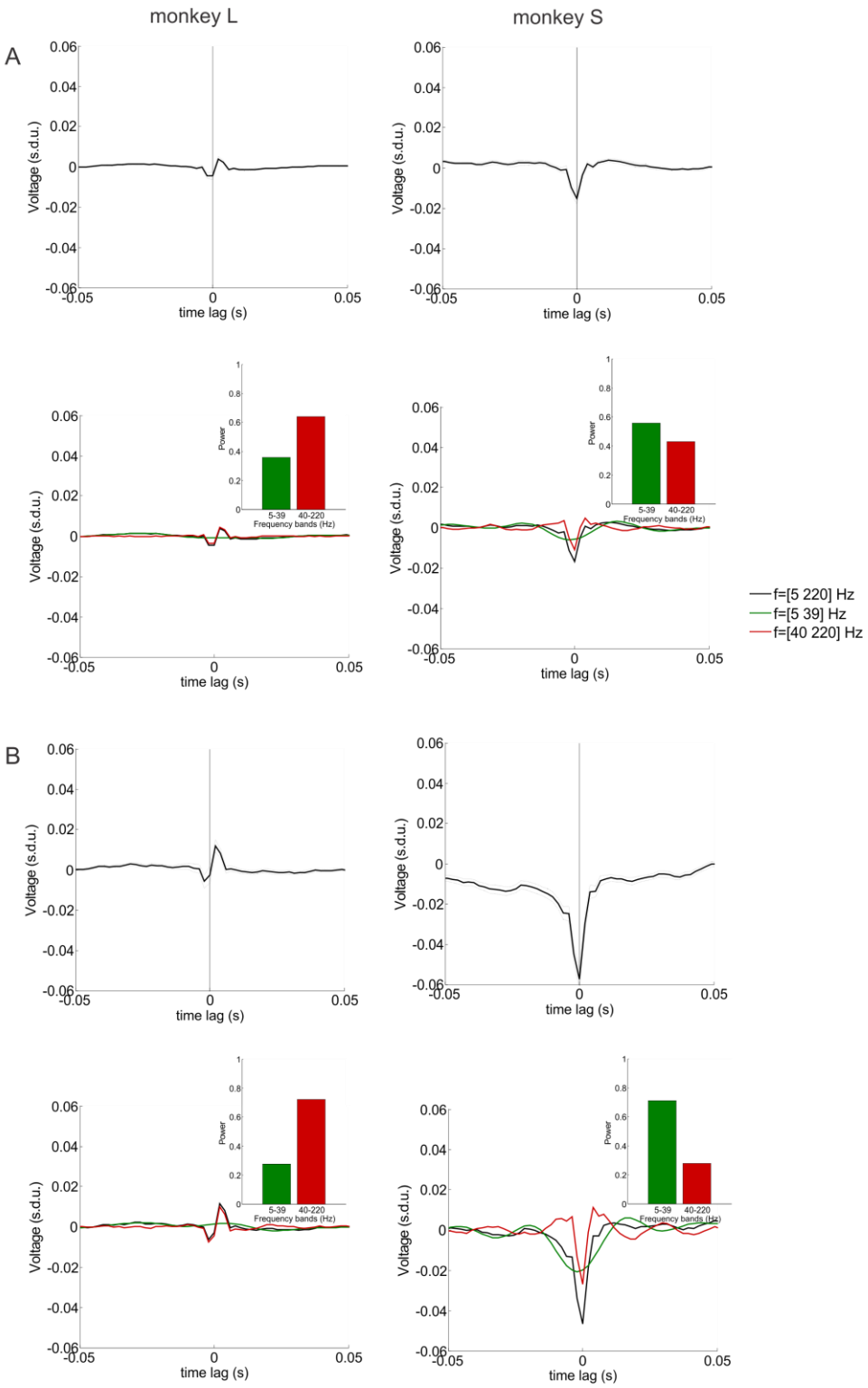

Fig. 6. Averages across all electrodes of W-K linear filters obtained with MUA (Fig. 6A) and spike trains (Fig. 6B), in Reward Expectation epoch, for monkey L (left) and monkey S (right). For each electrode, half of the trials were used to compute the W-K filters. Green lines: component of W-K kernel obtained by filtering in [5 39] Hz frequency range; red lines: component of W-K filter in [40 220] Hz. Inset bar plots: power of the two components of the filter, normalized to the power of unfiltered kernel

As previously disclosed, results obtained in Cue Expectation and in Reward Expectation epochs are strongly different for the two monkeys, and are separately reported. Figure 5 shows W-K linear filters obtained with MUA (Fig. 5A) and spike trains (Fig. 5B), in Cue Expectation epoch of the trial, for respectively monkey L (left) and monkey S (right). Also in Cue Expectation epoch we obtained filters from spike trains that are similar to filters from MUA. Monkey L presents filters with a low frequency modulation as strong as the Movement but with opposite sign, whereas filters computed from monkey S have a flatter shape with a higher power in the low frequency band. Filter computed in Reward Expectation epoch (Fig. 6) are similar to the ones obtained in the Cue Expectation epoch, but with opposite results for the two animals: monkey L (left panels) presents a flat kernel with a high modulation in the high frequency band, whereas filters computed with monkey S data (right panels) show a higher modulation in low bands.

For each electrode we computed W-K linear filters and we tested LFP estimation performance by computing the Pearson's correlation coefficient (r, Estimation Accuracy) between LFP and its linear estimate, $LFP_{\mathrm{est}}(t)$. Figure 7 shows the epoch specific, average Estimation Accuracy ($\bar{r}$) and SEM. Figure 7A reports results for Inter Trial and Movement epoch, and the average is computed across all monkeys, all electrodes and movement conditions. Middle and lower panels show results obtained in Cue Expectation epoch (Fig. 7B) and in Reward Expectation epoch (Fig. 7C), averaging across electrodes and movement direction, for monkey L and S. Left and right panels refer to measures from filters and convolutions with, respectively, MUA and spike trains. If W-K filters and convolutions are computed with MUA, we tested the statistical significance of $\bar{r}$ by generating a white noise signal with the same mean and standard deviation of the experimental MUA and by computing linear filters and Estimation Accuracy (black dots) from this artificial signal. When linear estimation is computed using spikes, we tested the statistical significance of $\bar{r}$ generating random spike times with the same mean firing rate of the experimental ones and Poisson distribution.
Estimation Accuracies computed using MUA and spike times are similar for Inter Trial and Movement epochs. Minimum values are obtained in Inter Trial epoch ($\bar{r} = 0.076 \pm 0.02$ and $\bar{r} = 0.047 \pm 0.02$, for, respectively, MUA and spikes), Movement epoch shows maximum Estimation Accuracies ($\bar{r} = 0.27 \pm 0.01$ and $\bar{r} = 0.26 \pm 0.01$, for, respectively, MUA and spikes). On average, the linear estimation of LFP from linear

filters with our data led to a smaller accuracy respect to previous results from Rasch and coworkers, who found an average value $\bar{r} = 0.36 \pm 0.15$. Our measures can be explained considering that Rasch performed estimation on stationary signals of time duration up to 240s, whereas, because of the interplay of different behavioral states in countermanding task, we could only assume stationarity in shorter time epochs, ranging between 200 and 600 ms, which likely led to a noisy filter and to a worse estimation.

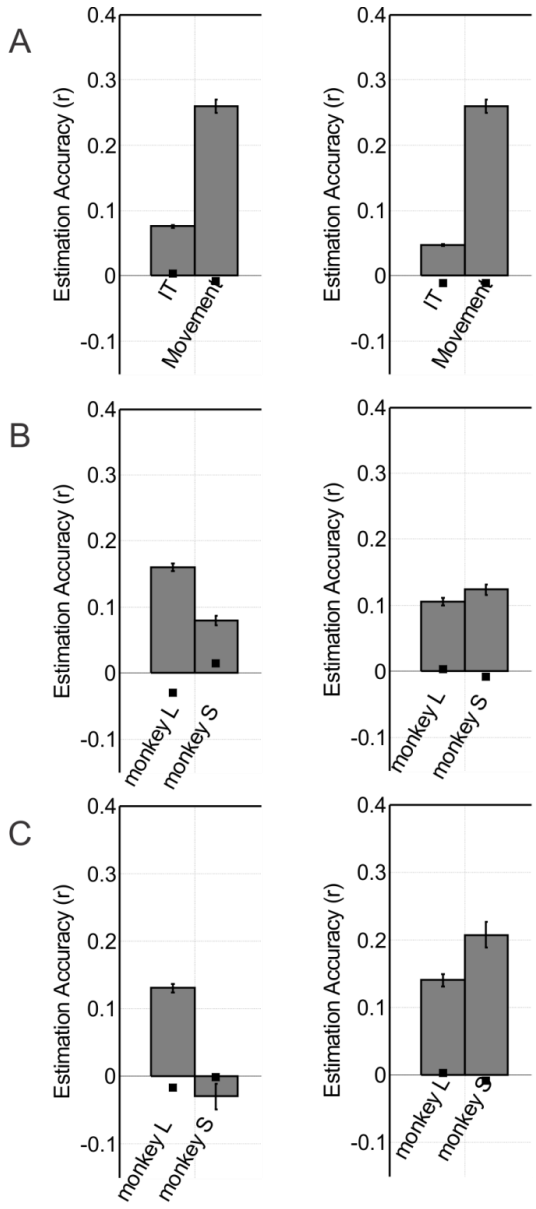

Fig. 7. Mean and SEM of Estimation Accuracy ($\bar{r}$). Figure 7A: results for Inter Trial and Movement epochs, averaging across all monkeys and all electrodes. Figure 7A and 7B: results for, respectively, Cue Expectation and Reward Expectation epochs, averaging across all electrodes, separately for monkey L and S. Left panels :mean Estimation Accuracies obtained using spike trains, black dots point out $\bar{r}$ obtained using Poissonian spike trains with the same mean firing rate of the experimental ones, right panel: mean Estimation Accuracies obtained using MUA. Black dots refer to $\bar{r}$ generated with a white noise signal with the same mean and standard deviation of the experimental MUA.

To further check the variability of linear filters depending on the behavioral state, we applied a kernel obtained in a specific epoch of the trial to estimate LFP of different epochs.

Figure 8A shows mean and SEM of Estimation Accuracy across all electrodes and directions, using filters obtained and convolved with MUA. The same analysis computed with spike times is shown in Figure 8B. We show results for monkey L in the first rows of Figure 8A and 8B, results for monkey S in second rows of Figure 8A and 8B. For each electrode, we computed $\bar{r}$ by applying Inter Trial (middle panels) and Movement (right panels) kernels to estimate LFP of the remaining trial epochs. We used a t test ($p<0.05$, one-tail t test, stars in the plots) to check if $\bar{r}$ significantly decreases respect to values computed using same epoch to obtain filters and estimate LFP (showed in left panels). The results claim that a significant decrease in $\bar{r}$ is obtained in 19 epochs (over 24), some epochs show a $\bar{r}$ which is not significantly different with respect the ones obtained with random processes (black dots) and in two cases we obtained a significantly negative Estimation Accuracy. These observations seem confirm that W-K filter temporal profiles remarkably depend on the trial epoch of the task.

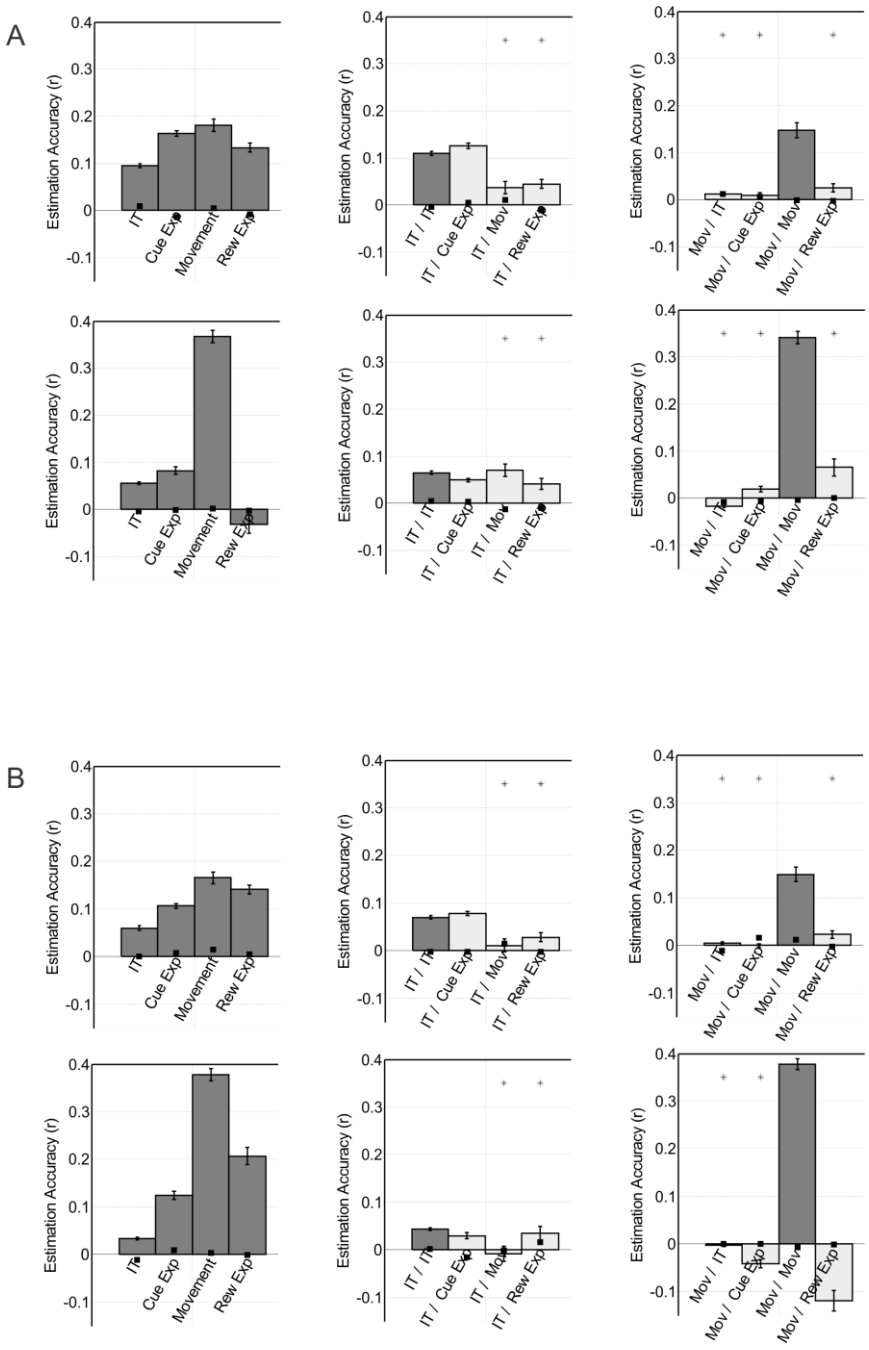

Fig.8. Estimation Accuracy computed convolving LFP in a specific epoch with W-K filter of a different epoch. Fig. 8A: W-K filters obtained and convolved with MUA. Results for monkey L and S are shown, respectively, in first and second row. Left panels: mean and SEM, across all electrodes, of Estimation Accuracies of different epochs of the trial; middle panels: mean and SEM of Estimation Accuracy computed convolving spike trains of each specific epoch with W-K filters of Inter Trial epoch; left panels: same analisys using filters of Movement epoch. A t test ($p<0.05$, *) was performed to evaluate whether $\bar{r}$ of middle and right panels were significantly lower than $\bar{r}$ in the left panels. Fig. 8B: W-K filters obtained and convolved with spike trains, same conventions of Fig. 8A.

2.2. Phase relationship between LFP and spiking activity

Because W-K filter contains information on the relationship between LFP and spikes it can be useful to provide insights into different network dynamics. Studying LFP rhythms captured in filters we can infer if a spike occurs preferentially at certain phase of LFP oscillations, and the strength of phase locking can be inferred by filter magnitude. Furthermore, positive and negative non-phase locked rhythms in LFP will cancel each other in the average, giving only the component of LFP that is phase locked to the spikes (Ray, Hsiao et al. 2008; Ray and Maunsell 2011)

To address the problem of how different LFP components can be locked in phase with spiking activity we studied phase-amplitude coupling between LFP and MUA as well as phase of LFP at spike times.

Phase-amplitude coupling (or nesting) is a specific type of interaction of rhythms in different frequency bands, in which the amplitude of high-frequency oscillations is modulated by the phase of low-frequency rhythms (Tort, Komorowski et al. 2010). Phase-amplitude coupling has been suggested to be involved in attentional selection and sensory selection (Schroeder and Lakatos 2009), according to a mechanism in which the phase at the time an input arrives in the cortex will determine whether it is attenuated or amplified. It has been also reported that phase of theta frequency of LFP at spikes times plays an important role in structuring and facilitating interaction between neurons in different brain regions during tasks involving memory (Lee, Simpson et al. 2005) and the same "facilitating" role was hypothesized to be carried out by synchronization between spikes and LFP oscillatory activity under 40 Hz, in motor cortex of monkeys (Murthy and Fetz 1996).

We filtered LFP with a bandwidth step of 5 Hz and computed the instantaneous LFP phase, where the phase range $[0\ 2\pi]$ is binned with $\pi/16$ step. To study the phase-amplitude coupling, we computed, for each electrode and LFP frequency band, the distribution of MUA amplitudes as a function of the LFP phase, mediating MUA amplitudes in each phase bin. We computed the normalized amplitude distribution, P_a , by dividing each bin value by the sum over the bins, so that the integral of P_a over the whole phase range is one. Similarly, for each electrode and LFP frequency band, we

computed the distribution of spike times as a function of the band-passed LFP phase and the normalized spike times distribution, P_s .

Figures 9A-B show, for Inter Trial and Movement epochs, the mean normalized phase-amplitude distribution, $\bar{P}_a$, as the average across all electrodes and monkeys of the normalized phase-amplitude electrode-specific distribution P_a. Figures 9B-C show the same results obtained with spike times distribution, $\bar{P}_s$.

Figures 10A-B show the mean normalized phase-amplitude distribution across all electrodes, $\bar{P}_a$, separately for monkey L and S, in Cue Expectation epoch. Similarly, Figures 10B-C show $\bar{P}_s$. Figure 11 is analogous to Figure 10, for Reward Expectation epoch. On the right of the lower panels is shown the sinusoidal convention used for phase, which is cosine type.

To measure the amount of phase locking, for each electrode and for each frequency interval we estimated modulation index (MI) as a measure that quantify the deviation of P_a (or P_s) from the uniform distribution, MI assumes values between 0 and 1, the former is related to a uniform distribution, the latter happens if P_a is a Dirac-like distribution. We also performed a statistical control analysis on MI through a bootstrap method with N=100 surrogate MI values. For each frequency band, we considered P_a (or P_s) significantly different from the uniform distribution if its MI exceeds 99% of surrogate MI.

If P_a or P_s are significantly not uniform, we infer the number of modes of the distribution to check for unimodality or bimodality. The upper panels of Figures 9-11 show, for each frequency band, percentages of electrodes with P_a significantly different from the uniform distribution. In grey are shown percentages of electrodes with unimodal distribution, in black percentages of electrodes with P_a significantly bimodal.

For each frequency step, we computed $\overline{\mathrm{MI}}$, as the MI of mean distributions $\bar{P}_a$ and $\bar{P}_s$, and its standard deviation over frequency. In order to estimate the numbers of modes of $\bar{P}_a$ or $\bar{P}_s$ at those frequency where $\overline{\mathrm{MI}}$ is high, we set a threshold value of two standard deviations. In the middle panels of Figures 9-11 we report, for each frequencies with significant $\overline{\mathrm{MI}}$, the numbers of modes estimated for $\bar{P}_a$ or $\bar{P}_s$, showing, in grey and in black, frequencies with distribution respectively, unimodal or bimodal. In lower panel

we also reported, for each frequency, the mean phase values, with colors according to the described convention.

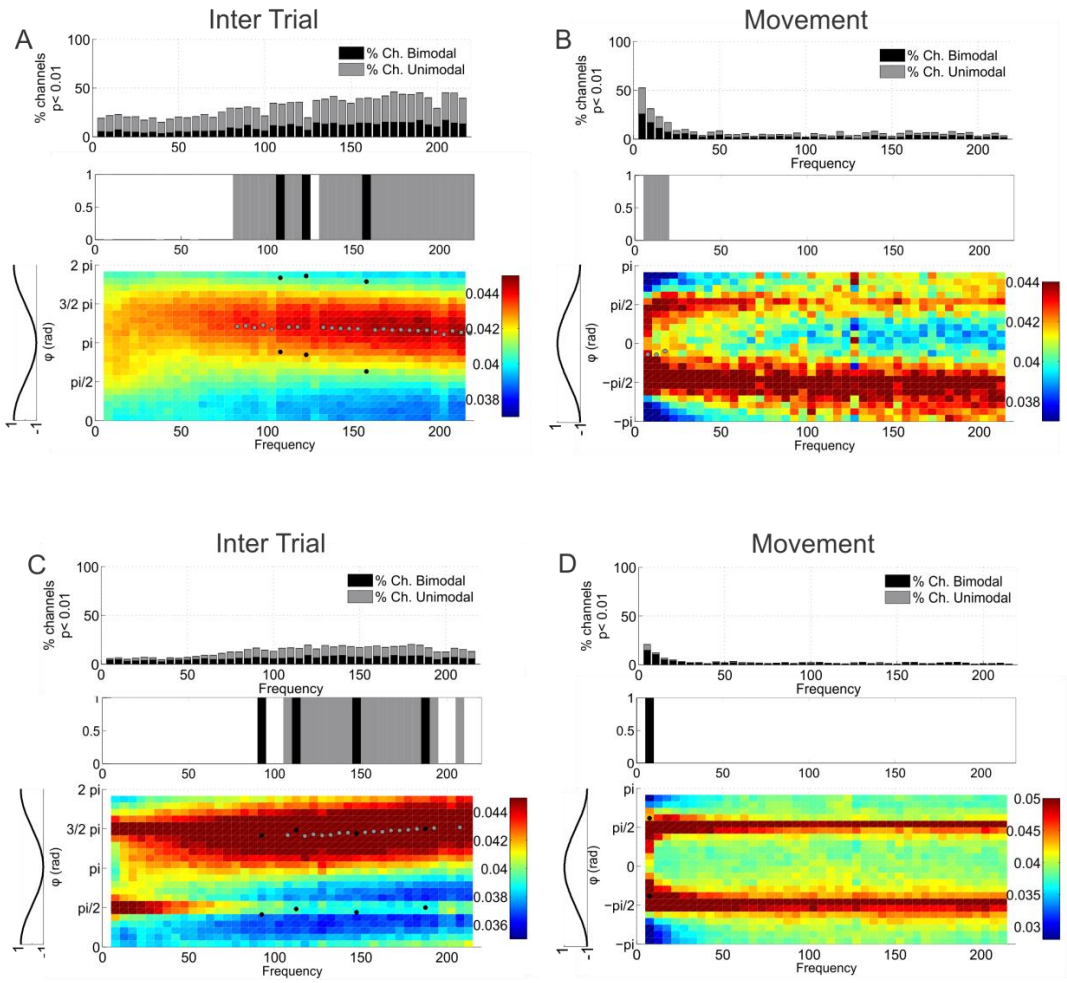

Fig. 9. Phase relationship between LFP and spiking activity in Inter Trial and Movement epochs. Fig. 9A and 9B: lower panel: mean normalized phase-coupling distribution, $\bar{P}_a$, between band-limited LFP and MUA, computed by averaging single electrode P_a across all electrodes and monkeys (on the right is shown the sinusoidal convention used for phase, which is cosine type, notice the different phase range used in Movement epoch); upper panel: for each frequency band, percentages of electrodes with P_a significantly different from the uniform distribution, grey bars: percentages of electrodes with unimodal distribution, black bars: percentages of electrodes with P_a significantly bimodal; middle panel: number of modes estimated for $\bar{P}_a$, shown for frequencies with significant modulation index $\overline{\mathrm{MI}}$, grey and black bars refer to significantly unimodal or bimodal $\bar{P}_a$. Dots in lower panel report, for each frequency with significant$\overline{\mathrm{MI}}$, mean phase values, with colors according to the described convention. Fig. 9C and 9D: phase of band-limited LFP at spikes times, same conventions of Fig. 9A and 9B.

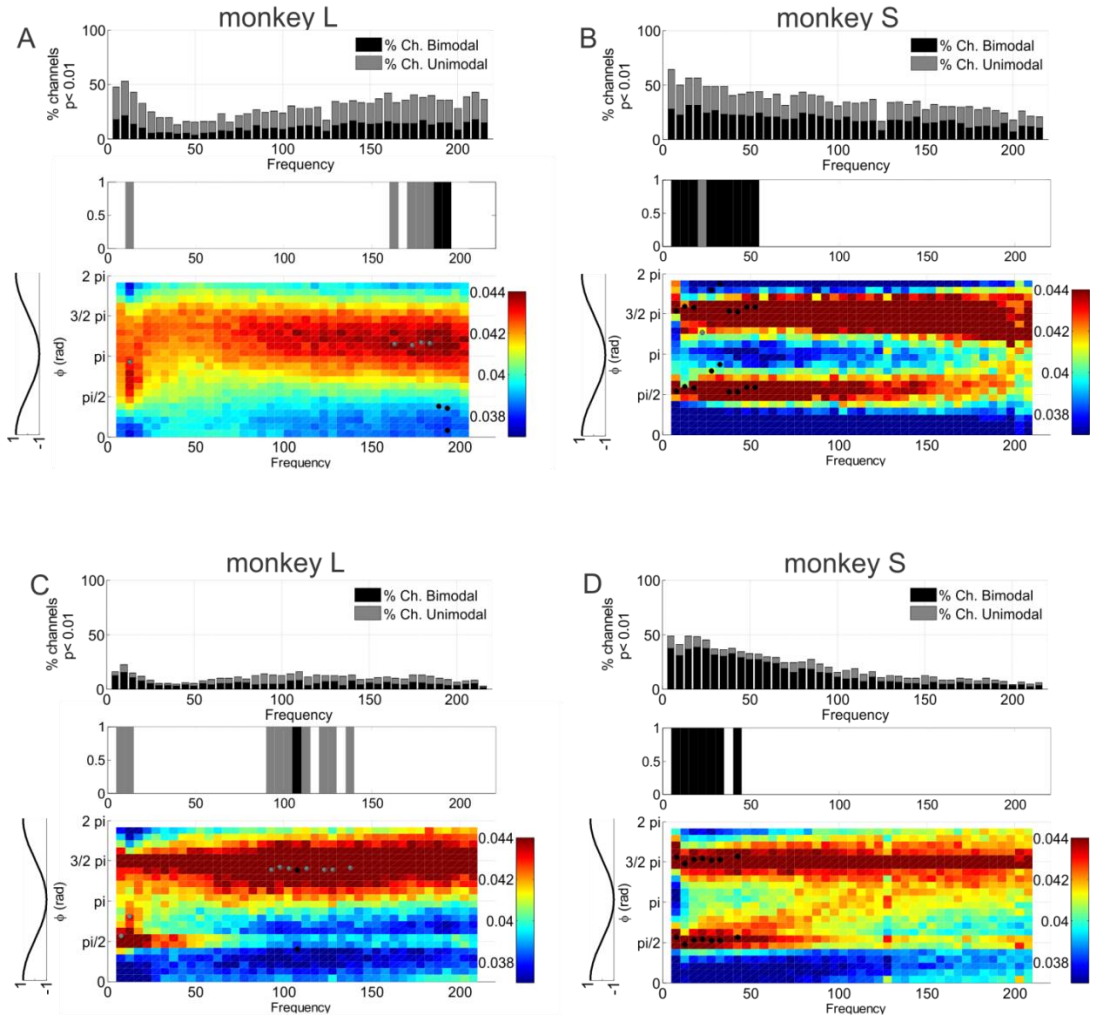

Fig. 10. Phase relationship between LFP and spiking activity in Cue Expectation epoch. Fig. 10A and 10B: lower panel: mean normalized phase-coupling distribution, $\bar{P}_a$, between band-limited LFP and MUA, computed by averaging single electrode P_a across all electrodes; showing separately results for monkey L (Fig. 10A) and monkey S (Fig. 10B); upper panel: for each frequency band, percentages of electrodes with P_a significantly different from the uniform distribution, grey bars: percentages of electrodes with unimodal distribution, black bars: percentages of electrodes with P_a significantly bimodal; middle panel: number of modes estimated for $\bar{P}_a$, shown for frequencies with significant modulation index $\overline{\mathrm{MI}}$, grey and black bars refer to significantly unimodal or bimodal $\bar{P}_a$. Dots in lower panel report, for each frequency with significant $\overline{\mathrm{MI}}$, mean phase values, with colors according to the described convention. Fig. 10C and 10D: phase of band-limited LFP at spikes times, same conventions of Fig. 10A and 10B.

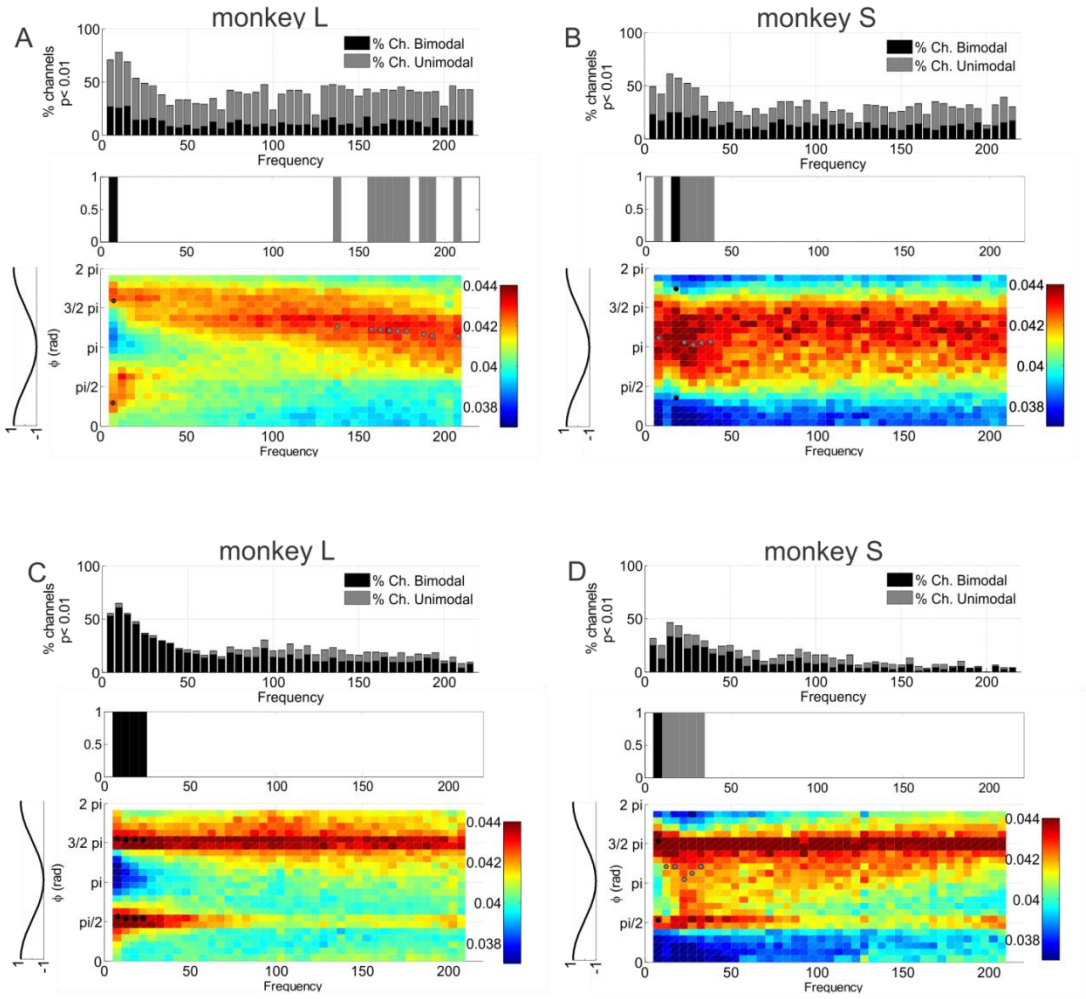

Fig. 11. Phase relationship between LFP and spiking activity in Reward Expectation epoch. Same convections of Fig 10.

As previously claimed, our hypothesis is that LFP components coupled with higher spiking activity will be captured in W-K filters. Inter Trial epoch (Fig 9A and 9C) shows a significant, unimodal phase locking at $\varphi = \pi$, which corresponds to the trough of LFP oscillation, can be recognized in W-K filter (Fig 4A and 4B, left panels). In Movement epoch, phase locking is significantly modulated only below 20 Hz (Fig 9B and 9D). Furthermore, MUA and spikes have their preferred phase at $\varphi = 0$, which corresponds to the peak of the underlying LFP rhythm, and the same profile can be recognized in W-K Movement filters (Fig 4A and 4B, right panels).

As previously discussed in linear estimation of LFP, results obtained in Cue Expectation and in Reward Expectation epochs are strongly different for the two monkeys, and must be reported separately. Similarly to what is shown for temporal profiles of W-K filters, monkey L and S yield to opposite results, with a phase distribution which is unimodal and strongly modulated in low frequency band (<50 Hz), for monkey L in Cue Expectation epoch and monkey S in Reward Expectation epoch. Similarly to epochs previously analyzed, low frequency phase locking at $\varphi = \pi$ is reflected in temporal profiles of W-K filters (Fig. 5, left panels and Fig. 6, right panels).
Finally, phase distributions for monkey L in Reward Expectation and monkey S in Cue Expectation are very similar, and show a modulation over all frequencies with a bimodal distribution with peaks at $\varphi = \pi/2$ and $\varphi = 3\pi/2$. Our hypothesis is that this "double locking" can average out both LFP components, leading to a flat W-K filters (Fig. 5, right panels and Fig. 6, left panels). in spite of strong phase locking.

As earlier claimed, we argued that the two animals used two different strategies to correctly perform the task , monkey S quickly orient eye response towards the peripheral cue as soon it appeared, conversely, monkey L did not make saccades to the cue at its appearance, but moved the eyes just before executing the procrastinated arm movement. These different plans of actions can take into account of the differences in Cue Expectation epoch that can be so related to different level of attention that the two monkeys exerted waiting for the lateral cue.

2.3. Phase of LFP at spike times of different neuron classes

How a bimodal distribution of LFP phase at spike times can arise? A possibility might be that two different neural populations, both active in a specific epoch of the trial, lock to different LFP phases. This scenario was described in previous works (Hasenstaub, Shu et al. 2005), which in prefrontal cortex of ferrets found, for inhibitory and excitatory neurons recorded during periods of recurrent network activity, a strong relationship between the probability of discharge and the phase of the γ oscillation of LFP, with a different preferred phase for inhibitory and excitatory neurons and with the inhibitory cells discharging to a higher frequency rate than excitatory.

To test this hypothesis, on each trial epoch, we sorted spikes, previously obtained with a threshold procedure on high-pass filtered extracellular raw signal, assigning them to putative single neuron clusters. We averaged all spike waveforms in each cluster to obtain an average action potential for each putative neuron. Then we classified neurons according to the time duration of their action potential, measuring that as the time interval from the trough to the peak (ttp) of the waveform.

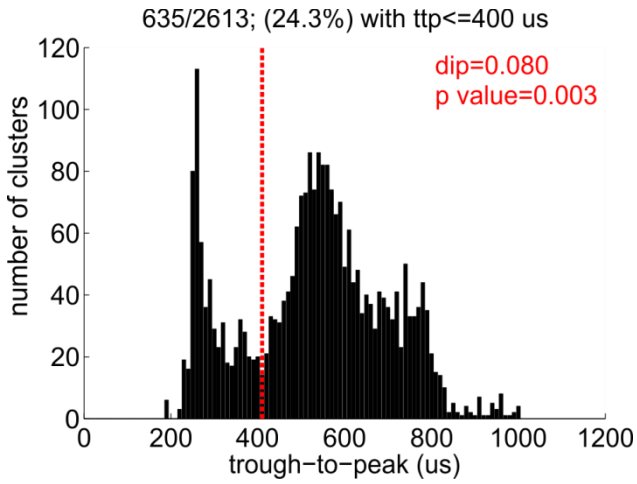

Fig. 12. Histogram of trough-to-peak (ttp) intervals of the 2613 putative neurons obtained with spike sorting method. A significant bimodality was found with a Hartigan's dip test ($p<0.01$). Putative inhibitory and excitatory neurons were classified on the basis of the two modes of the distribution: narrow-spiking, putative interneurons, having ttp in range [200 400] μs, broad-spiking, putative excitatory neurons, with ttp in range [400 900] μs.

We performed that analysis in each epoch of the trial and we obtained 2613 putative neurons, whose ttp is showed in Figure 12. An Hartigan's dip test was computed and we found a significant bimodality ($p<0.01$). According to previous studies (Mitchell, Sundberg et al. 2007; Song and McPeek 2010) we separated broad-spiking putative pyramidal neurons from narrow-spiking putative interneurons on the basis of the two modes of the ttp distribution, narrow-spiking neurons with ttp in the range [200 400] μs (24.3% of neurons) and broad-spiking neurons defined as those with ttp range [401 900] μs. The narrow-spiking neurons widths are longer than those found in visual cortex V4, which is 200 μs (Mitchell, Sundberg et al. 2007), but are comparable to the range of widths found previously in PMd cortex (Song and McPeek 2010) and in neurons related to saccades in FEF area (Cohen, Pouget et al. 2009).

Numbers of isolated neurons in each epoch are 1092, 203, 1117 and 201 for, respectively, Inter Trial, Movement, Cue Expectation and Reward Expectation. Percentage of narrow-spiking neurons differ in monkey L and monkey S: the former having 16%, 25%, 15% and 20% for, respectively, Inter Trial, Movement, Cue Expectation and Reward Expectation; the latter having 21%, 44%, 47% and 26% of putative inhibitory neurons. Percentages are in agreement with previous studies that estimated that the fraction of inhibitory neurons in the cortex is 20-30% (Mitchell, Sundberg et al. 2007), and also the over-representation of narrow-spiking neurons, found for monkey S in Movement and Cue Expectation epochs, was obtained in previous studies in PMd cortex (Kaufman, Churchland et al. 2010). Furthermore, according to other works which reported a higher level of spontaneous activity in putative inhibitory neurons(Song and McPeek 2010), we found that narrow spiking neurons exhibited a higher level of activity during Inter Trial epoch (mean, 8.5 spikes/s) than broad-spiking neurons (7.3 spikes/s, t test, p value<0.05). A significative higher firing rate for narrow-spiking neurons (mean 6.1 spikes/s) than broad-spiking neurons (mean, 5.2 spikes/s, t test, p value<0.05) was also found for monkey L in Cue Expectation epoch and in Reward Expectation epoch (12.4 spikes/s vs 6.8 spikes/s, t test, p value<0.05).

After having divided the whole putative single neuron population in two different classes of broad-spiking, putative pyramidal neurons and narrow-spiking, putative interneurons, we again computed linear estimation of LFP from spikes and phase of LFP at spikes times. We first performed the analysis for the whole unclassified population, to test if a smaller amount of spikes times, caused by spike sorting analysis and related rejection

process (as described in Methods chapter), could affect our results. Then we performed linear LFP estimation and phase analysis for each of the neuron classes.

Figures 13-15 show linear estimation analysis and phase distribution of LFP at spike times in different epochs of the trial. Figures 13 A and 13 B describe, respectively, Inter Trial and Movement epochs, and all results have been obtained by averaging across all electrodes and across both monkeys. Figure 14 and 15 show results obtained in Cue and Reward Expectation epochs and panels A and B refer to, respectively, monkey L and monkey S.

The arrangements of showed results is the same in each figure: left panels refer to data obtained from all putative single neurons, without separating respect to the ttp interval; right panels, upper and lower, show result of, respectively, narrow- and broad- spiking neurons. Bar plots report Estimation Accuracies for each neural population.

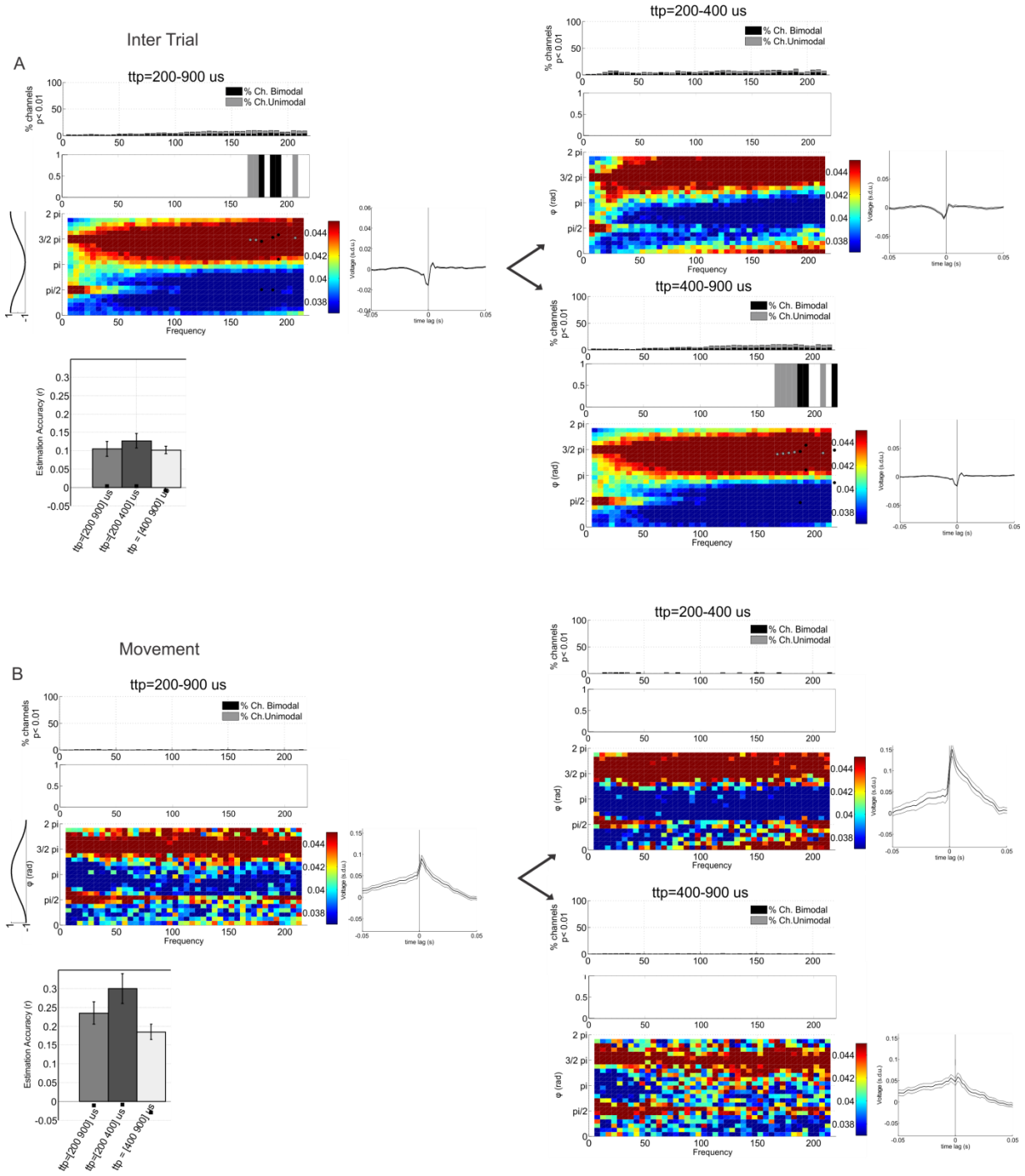

Fig. 13. LFP linear estimation and phase of LFP at spike times of different neuron classes, during Inter Trial (Fig. 13A) and Movement (Fig 13B) epochs. Results are obtained averaging across all electrodes. Left panel: results obtained with all putative single neurons, upper right panel: results obtained with neurons classified as putative inhibitory (ttp in range [200 400] μs), and lower right panel results obtained with neurons classified as putative excitatory (ttp in range [400 900] μs). Each figure shows, for each neuron class: W-K filter, Estimation Accuracy and phase distribution with the same convention of Fig. 9.

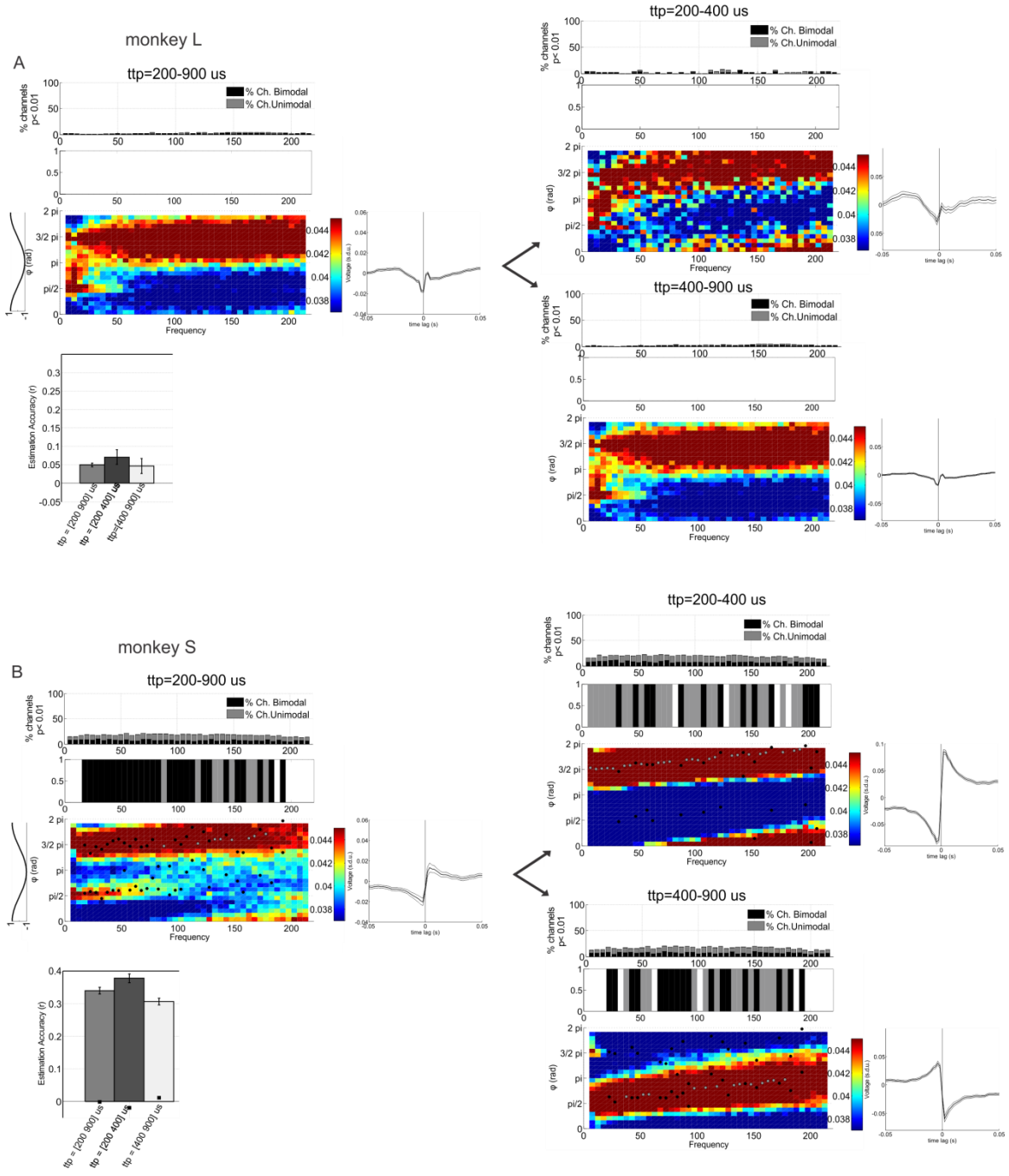

Fig. 14. LFP linear estimation and phase of LFP at spike times of different neuron classes, during Cue Expectation epoch, for monkey L (Fig. 14A) and monkey S (Fig 14B). Left panel: results obtained with all putative single neurons, upper right panel: results obtained with neurons classified as putative inhibitory (ttp in range [200 400] μs), and lower right panel results obtained with neurons classified as putative excitatory (ttp in range [400 900] μs). Each figure shows, for each neuron class: W-K filter, Estimation Accuracy and phase distribution with the same convention of Fig. 10.

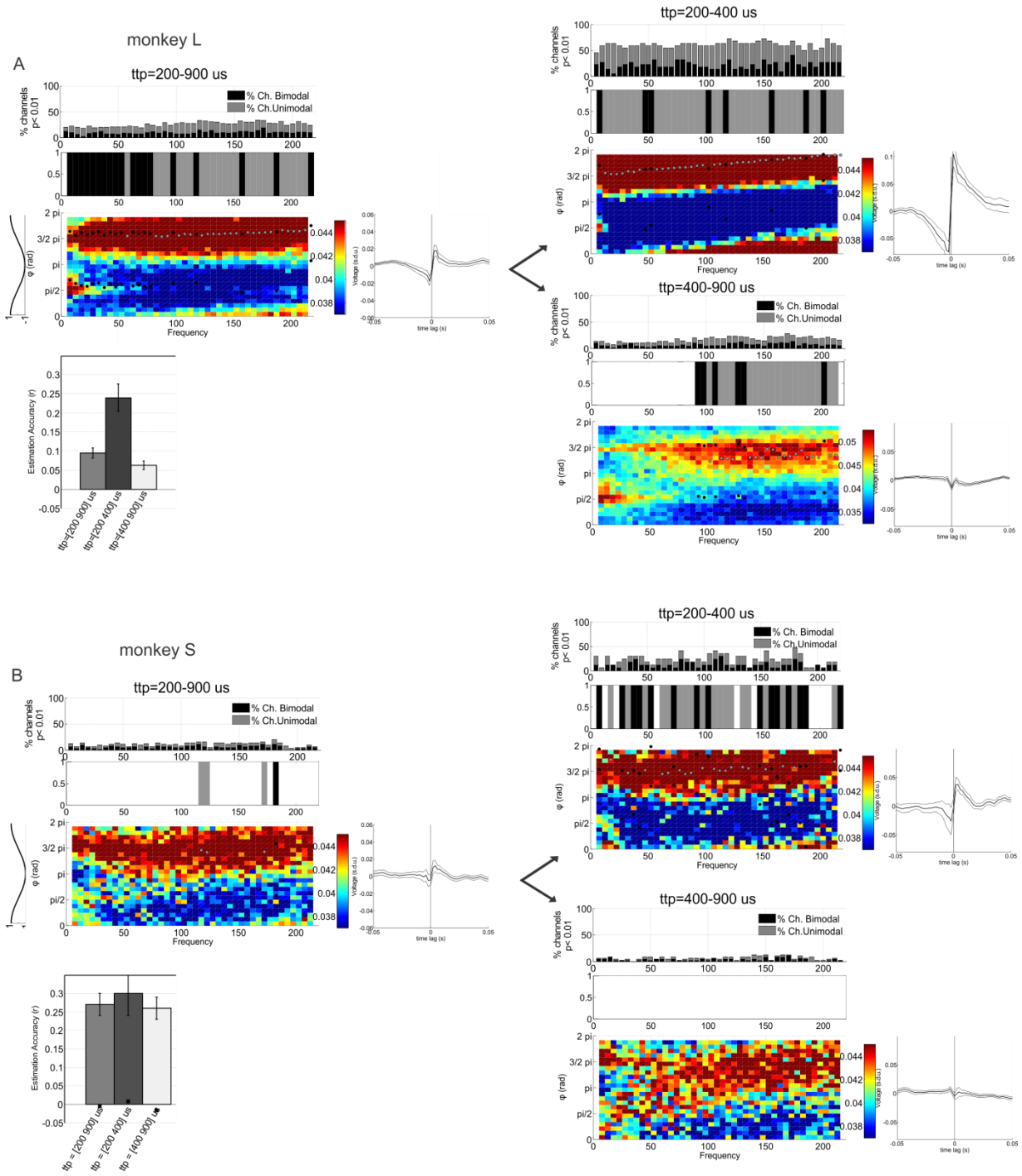

Fig. 15. LFP linear estimation and phase of LFP at spike times of different neuron classes, during Reward Expectation epoch, for monkey L (Fig. 15A) and monkey S (Fig 15B). Conventions like Fig. 14.

Accuracies of LFP estimations, temporal profiles of W-K kernels and distributions of LFP phase at spike times, obtained with unclassified, whole neural populations (left panels) do not considerable differ from previous analysis, even if a preponderance of $\varphi = 3\pi/2$ as preferred phase can be recognized in single neuron spiking activity, together with better perform in estimating LFP. In agreement to our hypothesis, according to which different neural populations discharge at different phases of LFP, this over-representation of spikes at $\varphi = 3\pi/2$ could be caused by a population with a higher firing rate, which had more chances to be effective in spike sorting process.

Results regarding LFP estimation and phase analysis in classified populations of narrow- and broad-spiking neurons strongly depend on the epoch of the trial. Distributions of phase of LFP at spike times in epochs with a unimodal distribution of phase such as Inter Trial (Fig 13 A), Cue Expectation for monkey L (Fig. 14 A) and Reward Expectation for monkey S (Fig 15 B) do not exhibit remarkable differences between narrow- and broad-spiking neurons, regarding phase distributions, filters profiles and Estimation Accuracies. However can be notice that putative interneurons show stronger phase locking, higher amplitudes for W-K filters and higher accuracies in LFP estimation, than the putative excitatory neurons.

In epochs with bimodal distributions of phase of LFP at spike times, such as Cue Expectation epoch for monkey S (Fig. 14B) and Reward Expectation epoch for monkey L (Fig. 15A), differences of preferred phase for narrow- and broad-spiking neurons become more important, with spikes of putative interneurons strongly locked to $\varphi = 3\pi/2$, which led to high amplitude W-K filters and Estimation Accuracies with the highest value (0.38 ± 0.02, for monkey S) or more than twice the unclassified neuron population.

Putative excitatory neurons have a preferred phase which differs of about π with respect to the preferred phase of putative interneurons. Broad-spiking neurons have a high probability of discharge at $\varphi = \pi/2$ in low frequency band of LFP (<50 Hz, Reward Expectation epoch of monkey L, Fig. 15A), but also over all LFP frequencies, as found in Cue Expectation epoch for monkey S, Fig. 14B.

These results are in agreement with previous studies which reported that attentional and arousal states strongly modulate spike timing of both excitatory and inhibitory neurons,

with the latter exhibiting higher firing rates and a higher degree of synchrony with LFP oscillations. (Hasenstaub, Shu et al. 2005; Mitchell, Sundberg et al. 2007).

4. Discussion

A common experimental approach to investigate the processing of sensory information (particularly used in visual and auditory systems) is to try to compute a function (functional, F) which permits to reconstruct a neural response y(t), from a stimulus x(t), according to the expression y(t)=F[x(t)]. In the traditional terminology this problem is known as "signal estimation" (Poor 1994). Usually, the functional F is the spike-triggered average of the stimulus, otherwise it can be a Wiener-Kolmogorov linear filter.

In a recent work, Rash and coworkers (Rasch, Logothetis et al. 2009) applied methods of signal estimation theory to LFP (x and y being in this case the spike train and the LFP respectively) and found that is possible to explain a significant fraction of the LFP time course from neural spiking activity. They also found that the functional F, which permits to reconstruct LFP from spikes, is general and does not change across different stimuli, electrode locations and subjects.

We are primarily interested in studying how the functional F , estimated as a stardard Wiener filter, changes depending on the behavioral state or the trial phases during the execution of a task: because F contains informations on the relationship between LFP and spikes, and LFP conveys information at the population level, such relationship can be useful to provide insights into different network dynamics occurring during the trial, both when the predictive value of F is high and when it is low; for example, the degree of LFP predictability from spikes might suggest a more local or distributed neural processing in the corresponding trial phase.

According to previous works (Ray, Hsiao et al. 2008; Ray and Maunsell 2011; Ray and Maunsell 2011), the functional F capture all activity that is locked to spikes. This includes events strictly associated to the spikes, such as presynaptic and post synaptic currents, which are recognizable as fast and sharp components with zero lag with respect to the spike time. Furthermore, F also contains all network oscillations, potentially arising from different neural populations, which are phase locked to spike times: if spikes occur preferentially at certain phases of LFP, those oscillations will be captured in the functional.

In contrast to previous works, that studied LFP-spikes functionals in sensory cortex (Ray, Hsiao et al. 2008; Rasch, Logothetis et al. 2009), we found that the low frequency component of F capturing neural oscillations, is not invariant but changes in a task which involve motor activity as well as more generic cognitive processes such asdifferent levels of arousal or attention. These results are not surprising, considering that several investigators reported that phase relationships between LFP and spikes are influenced by experimental conditions and involve sensory stimuli (Montemurro, Rasch et al. 2008; Rasch, Gretton et al. 2008), motor behavior (Murthy and Fetz 1996), memory processes (Lee, Simpson et al. 2005; Fell and Axmacher 2011) and attention (Schroeder and Lakatos 2009; Harris and Thiele 2011). It has been proposed that higher locking of spikes with respect to the LFP oscillation could help the synchronization between neurons of different brain regions, which can be facilitated (or attenuated) depending on the phase of LFP rhythms at which spikes preferably discharge.

More surprising was to find that functionals F between spikes and LFP not only change depending on experimental conditions, but also change depending on the subject. It has to be noted, however, that results in different monkeys are similar and robust in epochs of the task during which the activity of underlying network is direct to a precise task (e.g. arm movement) or is in a baseline mode.

Differences in functionals between monkeys concern only epochs that can involve attention, which could be typical of the subject or could be biased by different strategies used by the monkey to correctly perform the task. In order to separate individual features from more general aspects, a possible method can be to link the attentional state to some recognizable network features. A suitable signal could be represented, for example, by beta-band activity, that some works reported to be connected to expectancy of a forthcoming sensory event, or to attention- driven stimulus selection when priority is given to existing stimuli over new signals (Engel and Fries 2010).

We also found that a tight relationship between spikes and LFP can be not expressed in temporal profiles of functional F. If, in a specific epoch of the task, different neural populations are active, this multiple locking can average out rhythms that, otherwise, if only one population were active, would be captured in F; this also highlights the ambiguity possibly affecting population signals, as noted in the Introduction.

Our interpretation is supported by previous studies which reported, in rodents tested in a simpler context, that during periods of recurrent network activity different neural populations of inhibitory and excitatory neurons have strong locking to different phases of LFP (Hasenstaub, Shu et al. 2005).

By disentangling different populations of putative interneurons and putative excitatory neurons (but similar procedures could be applied to further sub-populations) we could so obtain functionals that clearly express and convey information on the relationship between LFP and spikes.

Finally, our results strongly suggest that considering behavioral states and dynamics of different neural populations can improve, without further technique advances, linear estimation of LFP from spiking activity.

Bibliography

Belitski, A., A. Gretton, et al. (2008). "Low-frequency local field potentials and spikes in primary visual cortex convey independent visual information." J Neurosci **28**(22): 5696-5709.

Boussaoud, D. (2001). "Attention versus intention in the primate premotor cortex." Neuroimage **14**(1 Pt 2): S40-45.

Buzsáki, G. (2006). Rhythms of the brain. Oxford ; New York, Oxford University Press.

Cohen, J. Y., P. Pouget, et al. (2009). "Biophysical support for functionally distinct cell types in the frontal eye field." J Neurophysiol **101**(2): 912-916.

Einevoll, G. T., C. Kayser, et al. (2013). "Modelling and analysis of local field potentials for studying the function of cortical circuits." Nat Rev Neurosci **14**(11): 770-785.

Engel, A. K. and P. Fries (2010). "Beta-band oscillations--signalling the status quo?" Curr Opin Neurobiol **20**(2): 156-165.

Fell, J. and N. Axmacher (2011). "The role of phase synchronization in memory processes." Nat Rev Neurosci **12**(2): 105-118.

Gabbiani, F. and C. Koch (1996). "Coding of Time-Varying Signals in Spike Trains of Integrate-and-Fire Neurons with Random Threshold " Neural Computation **8**(1): 44-66.

Grün, S. and S. Rotter (2010). Analysis of parallel spike trains. New York, Springer.

Harris, K. D. and A. Thiele (2011). "Cortical state and attention." Nat Rev Neurosci **12**(9): 509-523.

Hartigan, P. M. (1985). "Computation of the Dip Statistic to Test for Unimodality." Applied Statistics-Journal of the Royal Statistical Society Series C **34**(3): 320-325.

Hasenstaub, A., Y. Shu, et al. (2005). "Inhibitory postsynaptic potentials carry synchronized frequency information in active cortical networks." Neuron **47**(3): 423-435.

Holzmann, H. and S. Vollmer (2008). "A likelihood ratio test for bimodality in two-component mixtures with application to regional income distribution in the EU." Asta-Advances in Statistical Analysis **92**(1): 57-69.

Jones, T. A. (2006). "MATLAB functions to analyze directional (azimuthal) data - I: Single-sample inference." Computers & Geosciences **32**(2): 166-175.

Katzner, S., I. Nauhaus, et al. (2009). "Local origin of field potentials in visual cortex." Neuron **61**(1): 35-41.

Kaufman, M. T., M. M. Churchland, et al. (2010). "Roles of monkey premotor neuron classes in movement preparation and execution." J Neurophysiol **104**(2): 799-810.

Lee, H., G. V. Simpson, et al. (2005). "Phase locking of single neuron activity to theta oscillations during working memory in monkey extrastriate visual cortex." Neuron **45**(1): 147-156.

Liu, J. and W. T. Newsome (2006). "Local field potential in cortical area MT: stimulus tuning and behavioral correlations." J Neurosci **26**(30): 7779-7790.

Logan, G. D., W. B. Cowan, et al. (1984). "On the ability to inhibit simple and choice reaction time responses: a model and a method." J Exp Psychol Hum Percept Perform **10**(2): 276-291.

Logothetis, N. K., J. Pauls, et al. (2001). "Neurophysiological investigation of the basis of the fMRI signal." Nature **412**(6843): 150-157.

Mardia, K. V. and T. W. Sutton (1975). "On the modes of a mixture of two von Mises distributions." Biometrika **62**(3): 699-701.

Mattia, M., P. Pani, et al. (2013). "Heterogeneous attractor cell assemblies for motor planning in premotor cortex." J Neurosci **33**(27): 11155-11168.

Mirabella, G., P. Pani, et al. (2011). "Neural correlates of cognitive control of reaching movements in the dorsal premotor cortex of rhesus monkeys." J Neurophysiol **106**(3): 1454-1466.

Mitchell, J. F., K. A. Sundberg, et al. (2007). "Differential attention-dependent response modulation across cell classes in macaque visual area V4." Neuron **55**(1): 131-141.

Mitzdorf, U. (1987). "Properties of the evoked potential generators: current source-density analysis of visually evoked potentials in the cat cortex." Int J Neurosci **33**(1-2): 33-59.

Montemurro, M. A., M. J. Rasch, et al. (2008). "Phase-of-firing coding of natural visual stimuli in primary visual cortex." Curr Biol **18**(5): 375-380.

Murthy, V. N. and E. E. Fetz (1996). "Synchronization of neurons during local field potential oscillations in sensorimotor cortex of awake monkeys." J Neurophysiol **76**(6): 3968-3982.

Pesaran, B., J. S. Pezaris, et al. (2002). "Temporal structure in neuronal activity during working memory in macaque parietal cortex." Nature Neuroscience **5**(8): 805-811.

Poor, H. V. (1994). An introduction to signal detection and estimation.

Quiroga, R. Q., Z. Nadasdy, et al. (2004). "Unsupervised spike detection and sorting with wavelets and superparamagnetic clustering." Neural Comput **16**(8): 1661-1687.

Rainer, G. (2008). "Localizing cortical computations during visual selection." Neuron **57**(4): 480-481.

Rasch, M., N. K. Logothetis, et al. (2009). "From neurons to circuits: linear estimation of local field potentials." J Neurosci **29**(44): 13785-13796.

Rasch, M. J., A. Gretton, et al. (2008). "Inferring spike trains from local field potentials." J Neurophysiol **99**(3): 1461-1476.

Ray, S., S. S. Hsiao, et al. (2008). "Effect of stimulus intensity on the spike-local field potential relationship in the secondary somatosensory cortex." J Neurosci **28**(29): 7334-7343.

Ray, S. and J. H. Maunsell (2011). "Different origins of gamma rhythm and high-gamma activity in macaque visual cortex." PLoS Biol **9**(4): e1000610.

Ray, S. and J. H. Maunsell (2011). "Network rhythms influence the relationship between spike-triggered local field potential and functional connectivity." J Neurosci **31**(35): 12674-12682.

Rees, G., G. Kreiman, et al. (2002). "Neural correlates of consciousness in humans." Nat Rev Neurosci **3**(4): 261-270.

Schroeder, C. E. and P. Lakatos (2009). "Low-frequency neuronal oscillations as instruments of sensory selection." Trends Neurosci **32**(1): 9-18.

Song, J. H. and R. M. McPeek (2010). "Roles of narrow- and broad-spiking dorsal premotor area neurons in reach target selection and movement production." J Neurophysiol **103**(4): 2124-2138.

Spurr, B. D. and M. A. Koutbeiy (1991). "A comparison of various methods for estimating the parameters in mixtures of von Mises distributions." Communications in Statistics - Simulation and Computation **20**: 725-741.

Stark, E. and M. Abeles (2007). "Predicting movement from multiunit activity." J Neurosci **27**(31): 8387-8394.

Tort, A. B., R. Komorowski, et al. (2010). "Measuring phase-amplitude coupling between neuronal oscillations of different frequencies." J Neurophysiol **104**(2): 1195-1210.